Geochemistry 84 (2024) 126049

Contents lists available at ScienceDirect

Geochemistry

journal homepage: www.elsevier.com/locate/chemer

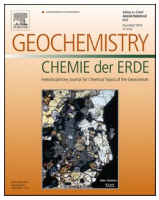

The bimodal Fii-A2-type and calc-alkaline volcanic sequence of the Aljustrel brownfield region, Iberian Pyrite Belt, SW Iberian Massif

João Lains Amaral [a,b,c,*], Ana Rita Solá [c], Telmo M. Bento dos Santos [a,b], Lorena Feitoza [a,b,d], Colombo Tassinari [e], Lourenço Crispim [a], Martim Chichorro [f], Mandy Zieger-Hofmann [g], Jessica Gärtner [g], Ulf Linnemann [g], João Gonçalves [h]

[a] Departamento de Geologia, Faculdade de Ciências da Universidade de Lisboa, Ed. C6, Piso 4, Campo Grande, 1749-016 Lisboa, Portugal
[b] Instituto Dom Luiz (IDL), Campo Grande, 1749-016 Lisboa, Portugal
[c] Laboratório Nacional de Energia e Geologia (LNEG), Bairro do Zambujal, Apartado 7586- Alfragide, 2610-999 Amadora, Portugal
[d] Departamento de Geologia, Instituto de Geociências, Universidade Federal de Roraima, Brazil
[e] Instituto de Geociências e Instituto de Energia e Ambiente, Universidade de São Paulo, Rua do Lago, 562, 05508-900 São Paulo, SP, Brazil
[f] GeoBioTec, NOVA University of Lisbon, Quinta da Torre, 2829-516 Caparica, Portugal
[g] Senckenberg Naturhistorische Sammlungen Dresden, Sektion Geochronologie, 01109 Dresden, Germany
[h] Almina - Minas do Alentejo, S.A., Algares, 7600-015 Aljustrel, Portugal

ARTICLE INFO

Handling Editor: Okay Çimen

Keywords:
Bimodal volcanism
Protracted magmatic setting
Geochemistry
Sr-Nd isotopes
U-Pb isotopes
VMS deposits
Variscan Orogeny

ABSTRACT

The Iberian Pyrite Belt (IPB) is a late Devonian – Early Carboniferous world-class polymetallic VMS province that includes significant Cu-(Sn)-Pb-Zn-(Ag) deposits of massive sulphides and feeder zones. The Aljustrel brownfield region contains one of the highest concentrations of ore in the IPB in 6 known deposits (Gavião, São João, Moinho, Algares, Estação and Feitais). To delve into the petrogenesis of the Aljustrel early Carboniferous (~355 Ma) felsic-dominated bimodal volcanism, new whole-rock trace elements and Sm—Nd isotopes, and U—Pb in zircon were obtained.

Based on Ga/Al and Y/Nb ratios, it is shown that Aljustrel felsic magmatism has the geochemical features of A2-type melts, typical of post-collisional and back-arc settings. U—Pb in zircon for a juvenile felsic volcanic rock point to antecrysts ages spanning from 387.9 to 366.6 Ma and a maximum emplacement age of 354.3 ± 2.6 Ma. These long-lasting melting events, present in both juvenile (ƐNdi = +1.79) and evolved felsic rocks (ƐNdi = −5.07), imply heterogeneous sources dominated by zircon-bearing igneous rocks. The Sm—Nd model ages are in accordance with previous Lu—Hf model ages in zircon, reinforcing that the isotopic variability is related to the same petrogenetic process.

Subordinated Aljustrel mafic rocks, coeval with the abundant felsic volcanism, show orogenic signatures, namely Nb-Ta-Ti negative anomalies and calc-alkaline affinities, whereas Sm—Nd isotopic data (ƐNdi = +1.54 to +5.48) points to variable to no contamination with crustal material. These geochemical results suggest derivation from an enriched mantle source modified by subduction metasomatism. In addition, the mafic rocks did not provide zircons for geochronological analysis, with the exception of one sample, in which a Concordia age of 402.1 ± 15.5 Ma was obtained from a single grain.

The combined geochemical signatures of mafic and felsic volcanic rocks suggest asthenospheric rise, but this solely does not explain the abundance of zircon antecrysts in the felsic rocks. Therefore, a geodynamic model that includes a continuous evolution from Devonian to Carboniferous times is inferred. This more complex and broader geodynamic model for the Iberian Pyrite Belt in which successive metal remobilization occurred after successive melting events, fits the present geochemical data and is more likely to explain why the Iberian Pyrite Belt is a unique metallogenetic province.

* Corresponding author at: Departamento de Geologia, Faculdade de Ciências da Universidade de Lisboa, Ed. C6, Piso 4, Campo Grande, 1749-016 Lisboa, Portugal.
E-mail address: jlainz@gmail.com (J.L. Amaral).

https://doi.org/10.1016/j.chemer.2023.126049
Received 30 May 2023; Received in revised form 19 November 2023; Accepted 22 November 2023
Available online 28 November 2023

1. Introduction

Volcanogenic Massive Sulphides (VMS) or Volcanic-Hosted Massive Sulphides (VHMS) are key polymetallic Cu-Pb-Zn-(Sn-Ag-Au) ore-bearing deposits that often develop in extensional geodynamic settings (Piercey, 2011), such as oceanic back-arcs or intracontinental rifts (Hannington et al., 2005). Extensional regimes may be formed in active, post-collisional and post-orogenic/anorogenic settings (Ishibashi et al., 2015; Schandl and Gorton, 2002; Zengqian et al., 2003). These deposits are often formed in deep seawater settings associated to bimodal volcanism, that drives sea water hydrothermal circulation, although the role of volcanism (and plutonism at deeper levels) and its influence on the bearing-ore fluids composition is usually unclear (e.g., in the Iberian Pyrite Belt: Barriga and Kerrich, 1984; Huston et al., 2011; Relvas et al., 2006; Tornos, 2006; Tornos et al., 2005; Yesares et al., 2023). Understanding the precise nature, geodynamic setting and timing of the magmatism hosting polymetallic giant VMS deposits (>200 Mt) is crucial to understand the formation of these deposits that can provide the critical raw materials necessary to fuel the global transition to a more sustainable society.

The Iberian Pyrite Belt (IPB) is a late Devonian-Early Carboniferous world-class VMS felsic-dominated province formed in a major intra-continental extensional event related to abundant bimodal magmatism after the onset of the oblique continental collisional between Laurussia and Gondwana (Azor et al., 2008; Chopin et al., 2023; Dias da Silva et al., 2018; Lains Amaral et al., 2022a; Munhá, 1983; Quesada et al., 2019; Silva et al., 1990; von Raumer et al., 2017). The nature of the mafic and felsic volcanism and the geodynamic setting of this province has long been discussed (Mitjavila et al., 1997; Munhá, 1983; Onézime et al., 2003; Rosa et al., 2004; Rubio Pascual et al., 2013; Thiéblemont et al., 1997; von Raumer et al., 2017). The occurrence of within-plate to volcanic-arc felsic and mafic volcanic rocks (Mitjavila et al., 1997; Thiéblemont et al., 1997) has favoured either a subduction-related or a transtensional-related intracontinental rifting setting (Martin-Izard et al., 2016; Onézime et al., 2003; von Raumer et al., 2017). Although specific geodynamic scenarios are still being debated, most authors agree that mafic and felsic magmatism were derived from diverse sources: a broadly mantellic origin for the former and a crustal origin for the latter. Munhá (1983) suggested a heterogeneous mantle source to account for the arc-like and alkaline basalts (see also Thiéblemont et al., 1997), whereas Mitjavila et al. (1997) claimed that a E- and N-MORB mixing source coupled with crustal contamination could explain the variability of basic magmatism in the IPB (see also Morais et al., 2020; Rosa et al., 2004). The source of the felsic volcanic rocks of the IPB have been placed at the upper, middle and even lower crust (Codeço et al., 2018; Donaire et al., 2020a; Rosa et al., 2009) of felsic-intermediate composition (Munhá, 1983) or involving amphibolites (Thiéblemont et al., 1997). Valenzuela et al., 2011a, considering Sm—Nd isotopic data, suggested a heterogeneous source composed of juvenile mafic rocks and more evolved rocks. The more juvenile Sm—Nd isotopic signature of the magmatic rocks relatively to the IPB sedimentary rocks has also been used to suggest a Meguma Terrane affinity for the IPB (Braid et al., 2011), which is in accordance with the Meguma-type zircon detrital U—Pb age patterns of the oldest known sedimentary rocks of the IPB of Middle-Upper Devonian age (Braid et al., 2011; Lains Amaral et al., 2022b).

Many questions still exist regarding the nature of the volcanism that led to the formation of the IPB. In this work, using new whole-rock trace elements and Sm—Nd isotopes, and U—Pb in zircon, we will discuss the petrogenesis of the felsic-dominated bimodal volcanic package of the giant Aljustrel VMS region, containing the orebodies of Gavião, Algares, São João, Moinho, Feitais, and Estação, totalling >300 million tons of sulphides. We present a petrogenetic model that attempts to explain the protracted igneous activity of the Aljustrel deposit, which may have promoted the successive metal remobilization and their anomalous concentration, making the IPB a unique metallogenetic province.

2. Geological context

The South Portuguese Zone (SPZ), the southwesternmost branch of the Iberian Massif (Fig. 1a), has been considered an exotic terrain (e.g., Silva et al., 1990) relatively to the rest of the Gondwanan Iberian Massif. This branch has fauna assemblages and zircon detrital age patterns that point to a Laurussian affinity (Braid et al., 2011; Lains Amaral et al., 2022b; Pereira et al., 2018). In the SPZ southern sector, the Iberian Pyrite Belt (IPB) (Fig. 1b), which is the subject of the present work, comprises the Phyllite-Quartzite Group (PQG) and the Volcanic-Sedimentary Complex (VSC). The PQG is a Middle-Upper Devonian shallow-marine clastic sequence (Mendes et al., 2018; Moreno et al., 1996), deposited in an epicontinental setting (Jorge et al., 2006; Oliveira et al., 2019). Its U—Pb detrital signatures point to Meguma affinity (Braid et al., 2011; Lains Amaral et al., 2022b), a peri-Gondwana terrane that is thought to have docked with Laurussia in the early Devonian (Van Staal et al., 2009). In contrast to the PQG, the Upper Devonian-Lower Carboniferous VSC is generally considered to have formed in a transtensional tectonic setting (Silva et al., 1990), marked by felsic-dominated bimodal volcanism (Munhá, 1983), exhalative and hydrothermal precipitation (Barriga, 1983; Schermerhorn, 1970), and detrital deposition, such as black-shales, siliceous shales and purple/green shales (Oliveira et al., 2019, 2004). The Baixo Alentejo Flysch Group (Fig. 1b), which overlaps VSC, is a middle Mississippian-early Pennsylvanian turbiditic sequence that resulted from the denudation of the Gondwanan and Laurussian crustal blocks (Rodrigues et al., 2015).

The IPB is one of the largest sulphide provinces in the world with >2500 million tons of sulphide-bearing minerals (Leistel et al., 1997; Conde and Tornos, 2020) and currently with 9 operations producing >500,000 tons per year of Copper and Zinc (Lains Amaral et al., 2024, in press). This metallogenetic province has been divided into two main sectors: i) the northern branch, where mostly early Carboniferous volcanic felsic rocks host the mineralization (e.g. Rio Tinto) with the massive sulphides being interpreted as replacement ore; and ii) the southern branch, where the massive sulphides are hosted in late Devonian black shales and felsic volcanic rocks, being interpreted as exhalative ores (Tornos, 2006).

The IPB felsic volcanic rocks are often coherent associated with monomitic breccias related to volcanic domes emplacement and its dismembering (e.g., autoclastic and re-sedimented facies), fiamme-rich breccias, interpreted as proximal pyroclastic events and, the more distal facies, occurring as fiamme-rich or crystal-rich sandstone-mudstones (Rosa et al., 2008; Valenzuela et al., 2011b). They are often dacitic to rhyolitic in composition (Oliveira et al., 2013; Thiéblemont et al., 1997). U—Pb zircon geochronology has been used to date the emplacement of felsic volcanic rocks from ~390 Ma to ~340 Ma (Barrie et al., 2002; Feitoza et al., 2023; Lains Amaral et al., 2021b; Mello et al., 2018; Paslawski et al., 2020; Pereira et al., 2021; Rosa et al., 2009). In some brownfield and greenfield mining districts (i.e., Neves-Corvo, Rio Tinto, Aljustrel and Rosário Anticline), the felsic rocks may contain significant antecryts population, spanning up to ~60 Ma before the emplacement age (Albardeiro et al., 2023; Lains Amaral et al., 2021b; Oliveira et al., 2013; Solá et al., 2015). In addition, rare xenocrysts have also been identified (Lains Amaral et al., 2021a; Rosa et al., 2009). The mafic rocks are subordinated to the felsic one, but basic magmatism can be relevant is some mining districts (e.g., Lousal, Rio Tinto) (Gisbert et al., 2021; Morais et al., 2020) and intermediate andesitic rocks are significant in the northern branch of the IPB (Munhá, 1983; Tornos et al., 2015). The coherent mafic levels occur as sills and lava flows, including pillow lavas, but may show ambiguous modes of emplacement (Donaire et al., 2020b; Rosa et al., 2010; Valenzuela et al., 2011a). In addition, mafic clast-supported breccia, mafic-sediment breccia and epiclastic sandstone and siltstone have also been identified in the belt (Conde and Tornos, 2020; de Mello et al., 2022; Gisbert et al., 2021; Munhá, 1983; Rosa et al., 2010). So far, basic rocks have not been dated by precise geochronological methods, such as U—Pb in zircon. Indeed,

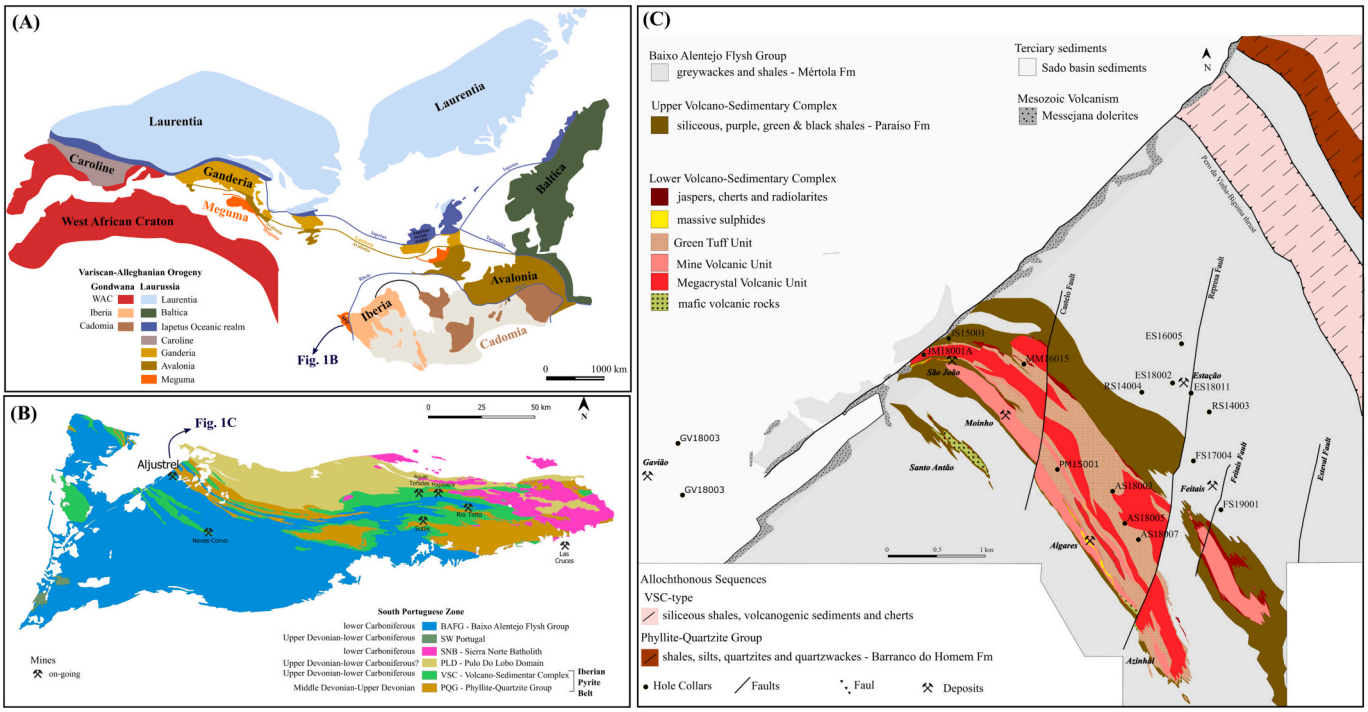

Fig. 1. a) Configuration of peri-Gondwanan terranes and main cratonic areas at the end of the Paleozoic (adapted from Lains Amaral et al., 2022b and references therein); b) Geological map of the South Portuguese Zone adapted from Lains Amaral et al., 2021b and references therein; c) Geological map of the Aljustrel adapted from Lains Amaral et al., 2021b and references therein.

researchers have not been able to recover zircons or baddeleyites from these mafic rocks (e.g., Luis Albardeiro, personal communication); thus, precise age of the mafic rocks is yet to be confirmed.

2.1. Aljustrel district

The Aljustrel district is a unique deposit as it is located in the northernmost sector of the southern branch (Lains Amaral et al., 2021b, Fig. 1b), being a volcanic-dominated deposit in which the massive sulphides have been interpreted as exhalative ores (Inverno et al., 2008).

The Aljustrel district is composed of six deposits: Feitais, Estação, Algares, Moinho, São João and Gavião (Andrade and Schermerhorn, 1971; Fig. 1c). The Aljustrel sequence is composed of a thick hydrothermally altered volcanic sequence of >250 m (Barriga and Fyfe, 1997) erupted at 359–353 Ma (Lains Amaral et al., 2021b) with rare levels of black shales (e.g., Silva et al., 1997) and impressive levels of massive sulphides and jasper at the top of the volcanic sequence (Barriga, 1983). The volcanic sequence mainly comprises felsic rocks (particularly proximal facies), but discrete mafic levels have also been observed (Leitão, 2009). This sequence has traditionally been divided into the unmineralized Megacrystal Volcanic Unit, the Mine Volcanic Unit, which hosts the economic mineralization, and are thought to have been laterally emplaced, and in the Green Tuff Unit, overlying the other two units (Andrade and Schermerhorn, 1971; Schermerhorn et al., 1987). In Aljustrel, the Variscan Orogeny is expressed by large-scale asymmetric folding related to thrusting. Tardi- to post-orogenic N-S to NE-SW faults, including the major Messejana Fault, truncate some of these structures (Barriga and Fyfe, 1997; Relvas et al., 2011).

3. Materials and methods

Sampling was carried out in 16 drill holes from the six deposits of Aljustrel deposits (São João, Moinho, Algares, Feitais, Estação and Gavião) and step-out drilling, totalling over 300 samples plus two surface samples. 114 representative samples of half core, NQ and HQ size and of ~0.3 to 0.8 m in length, were selected for geochemical analyses and sawed into ~2x2x3 cm blocks at the DG-FCUL (Departamento de Geologia da Faculdade de Ciências da Universidade de Lisboa, Portugal) and crushed to <1 cm, using a jaw crusher at LNEG (Laboratório Nacional de Energia e Geologia, Lisbon). Approximately 300 g of each sample was sent to the ALS Minerals laboratory in Seville, Spain, for pulverisation (laboratory code: PULP-31). Whole-rock geochemical analyses were carried out at the ALS Minerals laboratory in Dublin, Ireland under the package CCP-PKG01. Normalization values for primitive mantle ($\frac{PM}{N}$) according to Sun and McDonough (1989) and for chondrite ($\frac{C}{N}$) according to Nakamura (1974) have been used. Calculation of Eu/Eu* as well as binary and ternary plots were performed using GCDkit (Janoušek et al., 2006).

Twenty sealed laboratory pulverised reject samples were selected for Sm—Nd isotopes using ALS global services (laboratory code: Nd-ISTP01). The Sm—Nd isotopic analyses were carried out at the University of Alberta, Canada (see also Appendix SA1). Initial isotopic Nd values, Nd-depleted mantle model ages (TDM) and two stage model ages (2TDM) were calculated using the GCDkit Software (Janoušek et al., 2006). This software uses the value of 6.54×10^{-12} a^{-1} for the ^{147}Sm decay constant after Lugmair and Marti (1978). Further, it considers the $^{143}Nd/^{144}Nd$ and $^{147}Sm/^{144}Nd$ ratios of 0.512638 and 0.1967, respectively, according to DePaolo and Wasserburg (1979) for the Chondritic Uniform Reservoir (CHUR) to calculate ƐNd. For the calculation of model ages, the equations of Liew and Hofmann (1988) were used. 2TDM of published Sm—Nd isotopes (Donaire et al., 2020a; Luz et al., 2022; Mitjavila et al., 1997; Pascual et al., 2021; Valenzuela et al., 2011a) were recalculated using the same software. For published Lu—Hf isotopic data (Rosa et al., 2009), 2TDM and εHf were recalculated following the procedures established in Bento dos Santos et al. (2011). The $^{176}Lu - ^{176}Hf$ decay constant of 1.867×10^{-11} a^{-1}, $^{176}Hf/^{177}Hf_{CHUR} = 0.282785$ and $^{176}Hf/^{177}Hf_{CHUR} = 0.0336$ of Bouvier et al. (2008) for CHUR, $^{176}Lu/^{177}Hf_{DM} = 0.03976$ and $^{176}Hf/^{177}Hf_{DM} = 0.283238$ of Vervoort et al. (2018) for the Depleted Mantle (DM) were used. For the average $^{176}Lu/^{177}Hf$ of the crust the value of 0.015 after Griffin et al.

(2002) was used. The KDE plots of 2TDM ages were done with IsoplotR (Vermeesch, 2018).

Six half-core samples were selected for zircon separation. These samples were sawn and crushed (see above), followed by gridding and sieving (<250 μm) at DG-FCUL. Heavy mineral concentrates were obtained from the Wilfley table at DG-FCUL using a technique similar to that developed by Söderlund and Johansson (2002). Pyrite-rich concentrates were leached with nitric acid (n = 8) before hand-picking under a binocular microscope. Individual zircon grains were mounted, together with the TEMORA standard, in epoxy and then polished at the High-Resolution Geochronology Laboratory (GeoLab-SHRIMP) of the Institute of Geosciences, University of São Paulo, Brazil. Cathodoluminescence (CL) and backscattered electron (BSE) imaging, as well as 15 U-Pb analyses, were also performed at GeoLab-SHRIMP. Further details of the SHRIMP-IIe analytical procedures can be found in Sato et al. (2014) and Lains Amaral et al. (2021b). In addition, five single zircon grains were measured for U—Pb ages using LA-SF-ICP-MS techniques at the GeoPlasma Lab, Senckenberg Naturhistorische Sammlungen Dresden (Germany). Only two of these zircon grains showed a measurable signal, and only one gave a concordant age. For further details on analytical protocol and data processing see Appendix SA1 and Gerdes and Zeh (2006). Age and Concordia distance for each LA-ICP-MS or SHRIMP analysis, as well as radial plot and corresponding age calculations were performed with IsoplotR (Vermeesch, 2021a, 2018). Calculated age error in the main text and figures are in 1σ. Errors for individual analyses are presented in 1σ. The R software uses the values of 137.818 for $^{238}U/^{235}U$ ratio (Hiess et al., 2012), 0.155125×10^{-9} a^{-1} for ^{238}U decay constant (Jaffey et al., 1971) and 0.98485×10^{-9} a^{-1} for ^{235}U decay constant (Jaffey et al., 1971).

4. Results

4.1. Field observations and rock classification

The volcanic sequence of Aljustrel is a felsic-dominated sequence with sparse mafic rocks identified in the Algares and Gavião deposits. The felsic sequence has been divided into three main units: the Mine Unit, the Megacrystal Unit and the Green Tuff Unit. Considering the geochemical classification proposed by Barrett (2008) and Barrett et al. (2008), the latter two are geochemically distinguishable, and classified as RHY M and RHY C, respectively, while the Mine Unit is divided in two chemotypes: RHY A and B. Two more uncommon chemotypes have also been identified: RHY Z and RHY X.

The Mine Unit, which host the economic sulphides, is composed of coherent (Fig. SF1a), autoclastic (Fig. SF1b) and pyroclastic (Fig. SF1c) feldspar porphyritic felsic rocks (Barriga and Fyfe, 1997), as previously described by Leitão (2009), and has been divided by Barrett (2008) into two chemotypes (RHY A, RHY B). RHY A is spatial associated with massive sulphide lens in the Estação-Feitais deposits (Barrett et al., 2008), whereas in other deposits, massive sulphides are related to RHY B. Indeed, in this work, RHY A was only identified in the Feitais and Estação drill holes.

The very few high Al_2O_3/TiO_2 samples, classified as RHY Z, were also collected within the Mine Unit. This chemotype, however, was first identified by (Barrett, 2008) as spatial associated with RHY C or above it, in the lowermost sections of the Upper VS. The lack of a coherent stratigraphic position for RHY Z, the low expression of this chemotype, and even its relatively uncommon U-Pb-Th in zircon results (see Lains Amaral et al., 2021b), points that the RHY Z signature should be taken with caution.

Another chemotype defined by Barrett (2008), the more unusual RHY X chemotype, is also plagioclase-phyric (Fig. SF2). According to Barrett et al. (2008), RHY X may also contain quartz phenocryst in addition to the feldspar phenocrysts. Although a 200 m sequence of this chemotype has been identified in borehole ES16005, the chemotype RHY X has not yet been found hosting significant sulphides.

A visually distinctive crystal-rich volcanic unit, the Green Tuff Unit, which corresponds systematically to chemotype RHY C, is often found overlaying the massive sulphides and/or within the exhalative jasper-chert unit. In addition, these levels of plagioclase-quartz-rich volcanic rocks (Leitão, 2009) were also identified interlayered with the RHY M (Fig. SF3a) in hole AS18005 or, according to Leitão (2009), at the top of it. The crystal-rich unit is commonly massive and heavily altered by sericite (Fig. SF3a), which makes it difficult to determine their origin. Lains Amaral et al. (2021b) interpreted as coherent to autoclastic facies, however, the occurrence of jaspers and radiolarites (Leitão, 2009) may point out that, at least part of these levels may correspond to crystal-rich deposits. They may also contain abundant magnetite (Lains Amaral et al., 2021b). Chemotype RHY C also occurs at the bottom of three Algares drill holes (AS18007, A18005 and AS18003), comprising mostly pyroclastic units (Fig. SF3b), and rarely coherent levels (Fig. SF3c).

The Megacrystal Unit, composed of feldspar-quartz porphyritic volcanic rocks (Barriga and Fyfe, 1997; Fig. SF4), is unrelated to the sulphide mineralization and is visually distinguishable by the presence of feldspar megacrysts (Fig. SF4). This unit also presents various volcanic textures, but the fiamme-like textures, and other volcanoclastic alike features, are likely a product of hydrothermal alteration (Fig. SF4), and therefore, this massive unit is interpreted to be composed of coherent facies (see also Leitão, 2009).

In addition, mafic rocks were identified in Algares and Gavião deposits. The mafic rocks of Algares, in this work labelled as BAS VC, are often volcanoclastic rocks and may contain vesicular-rich clasts (Fig. SF5a–c), that have some resemblances with fluidal-clast breccias (Simpson and McPhie, 2001). In addition, strongly altered, relatively homogenous, mafic level was interpreted as a lava flow in hole PM15001 (Fig. SF5c). The contacts with the felsic units are often difficult to assert, but sharp contacts with either black shale (Fig. SF5a) or felsic rocks may occur. The mafic volcanic rocks that outcrop in the Algares area, in this work labelled as BAS O, are composed of lavas and volcanoclastic rocks. According to Leitão (2009) pillow-lavas also outcrop in this area. The Gavião mafic rocks, in this work labelled as BAS D and BAS DA, are massive volcanic levels, interpreted as intrusive sills, but the occurrence of ambiguous contacts, such as autobreccias and monomitic breccias (Fig. SF6a,c), associated to sulphide veining in hole GS18003, suggests that the emplacement of these albite sills (dos Santos, 2021) may have occurred soon after the formation of the host rocks. However, the sills do not show significant deformation (dos Santos, 2021; Relvas, 1991). Finally, a single purplish sill was also observed in the Gavião, labelled as BAS E, affected by abundant quartz veining. Considering the above, the mafic volcanism is both syn- and post-felsic volcanism.

It is also worth to mention that although mafic minerals were only identified in a section of a sill (Fig. SF6b), it is considered that mostly mafic minerals were not preserved, particularly in BAS VC (Fig. SF5), as elsewhere in the IPB (e.g., Gisbert et al., 2021; Valenzuela et al., 2011a, 2011b). Importantly, the mafic rocks, particularly BAS VC, BAS D-DA ad BAS E, form a coherent geochemical group, including the sample in which pyroxenes are preserved.

4.2. Whole-rock geochemistry and hydrothermal alteration

Hydrothermal alteration has been widely described in the volcanic rocks of the IPB (Morais et al., 2020; Munhá and Kerrich, 1980; Plimer and de Carvalho, 1982; Relvas et al., 2006; Sánchez-España et al., 2000), including the Aljustrel district (Barrett, 2008; Barriga, 1983; Relvas, 1991; Relvas et al., 2011). In the following subsections, the role of hydrothermal alteration in the composition of volcanic rocks is assessed. The whole-rock analyses are reported in Table ST1, supplementary data.

4.2.1. Major elements

The volcanic rocks of Aljustrel only show a good co-variation between SiO_2 and Al_2O_3 and LOI (Fig. 2). Overall, the mafic rocks are

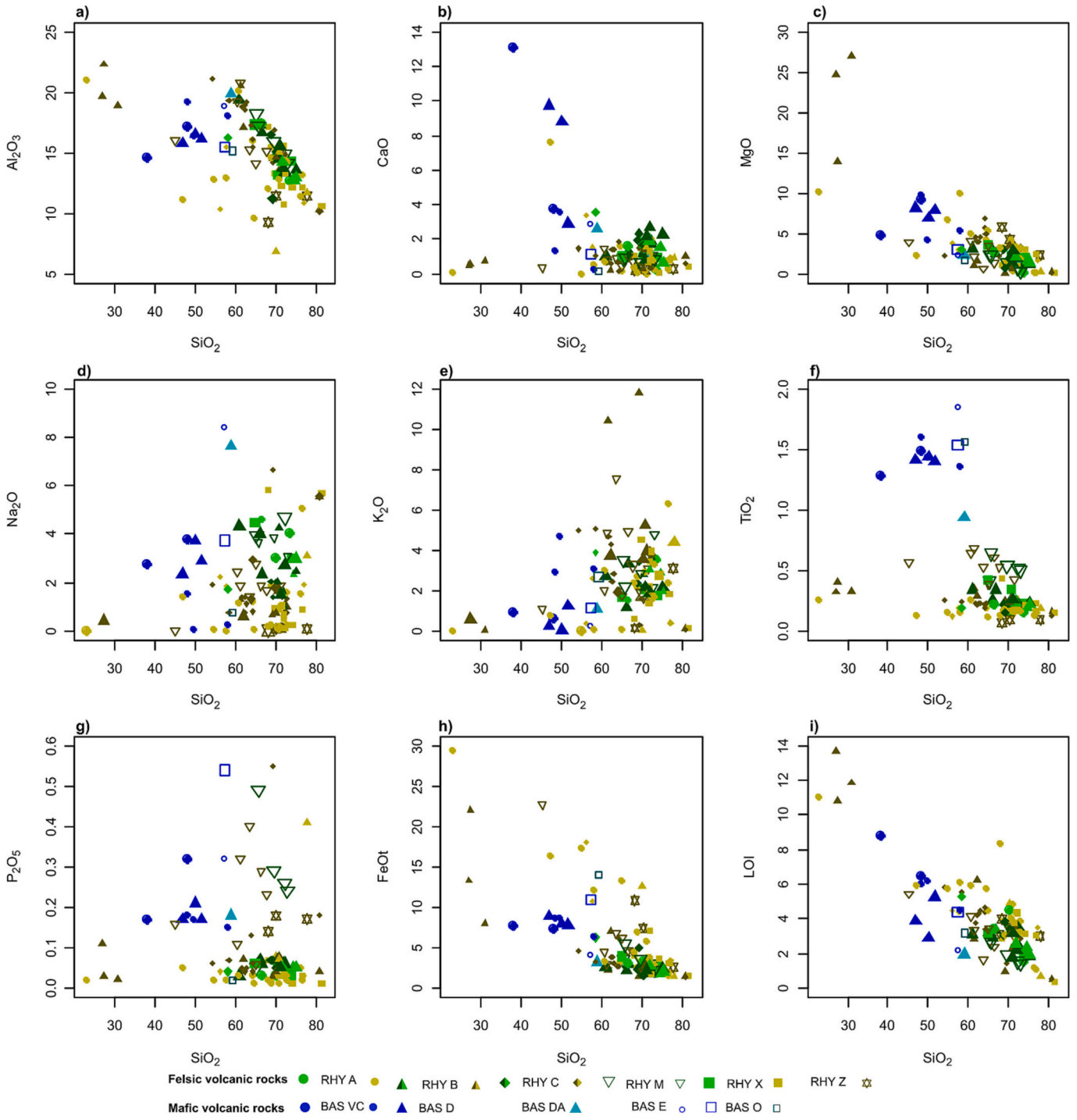

Fig. 2. Harker plots for the volcanic rocks of Aljustrel: SiO_2 vs. a) Al_2O_3; b) CaO, c) MgO; d) Na_2O; e) K_2O; f) TiO_2; g) P_2O_5: h) FeOt and i) LOI. Symbols as in Fig. 3.

discriminated against the felsic counterparts by their higher contents of CaO, MgO, TiO_2, P_2O_5 and FeOt, which may suggest major element mobility did not completely override the original composition. In contrast, strongly altered felsic volcanic rocks, such as chloritites, show exceptionally low silica contents (<35 %).

To attest the degree of hydrothermal alteration, the alteration parameters developed for VMS deposits, the chlorite-carbonate-pyrite index (CCPI) and the Ishikawa alteration index (AI) (Large et al., 2001) were used. The least altered box (Large et al., 2001) follows Gifkins et al. (2006) guidelines, thus a CCPI Index between 20 and 65 % for felsic rocks and between 65 % and 90 % for the mafic rocks are considered least altered. For the AI Index, the box plot is constrained between 20 and 65 %. The sampled volcanic rocks plot inside and outside of the least altered box, showing the variable intensity of hydrothermal alteration, particularly chloritization, sericitization and pyritization (Fig. 3a). In addition, the MFW diagram, which was initially developed to attest weathering of igneous rocks (Ohta and Arai, 2007), is also considered. The triangle alteration diagram corroborates the box plot and points that some of the mafic and felsic volcanic rocks are relatively least altered and closer to unaltered compositions (Fig. 3b). Both diagrams show that all the RHY Z samples collected are significant altered, only a few least altered samples of RHY A and RHY X were collected, and a sizeable portion of the mafic rocks collected plot in the basalt fields, pointing to relatively least altered compositions (Fig. 3a–b). The more altered BAS

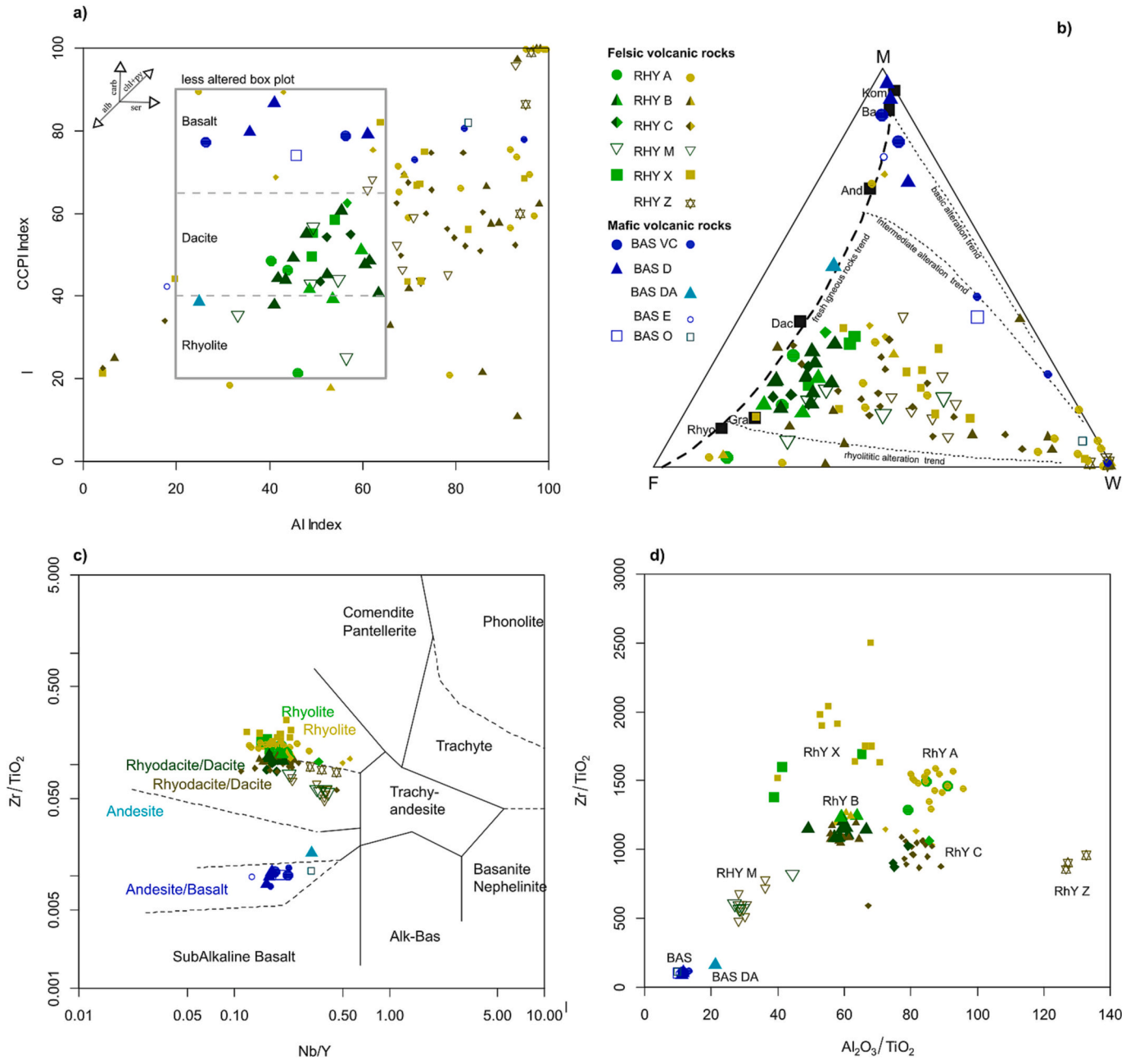

Fig. 3. Immobile element and alteration plots for the volcanic rocks of Aljustrel. a) Alteration index vs. CPP index, alteration diagram (Large et al., 2001). Alteration boxes adapted from Gifkins et al. (2006). Arrows represent the apparent main alteration trends. b) FMW diagram with igneous rocks and weathering trends (dashed lines) (Ohta and Arai, 2007). c) Zr/TiO_2 vs. Nb/Y, rock classification diagram (Winchester and Floyd, 1977). d) Al_2O_3/TiO_2 vs. Zr/TiO_2, chemotype classification after Barrett (2008) and Barrett et al. (2008). Bigger symbols, plotting inside the less altered box; smaller symbols plotting outside the less altered box. Dark blue: plotting in the andesite/basalt field; light blue: plotting in the andesite field; dark green, plotting in the rhyodacite/dacite field and in the less altered box; light green, plotting in the rhyolite field and in the less altered box; dark yellow, plotting in the rhyodacite/dacite field and outside the less altered box; light brown, plotting in the rhyolite field and in outside the less altered box. Close circle: RHY A or BAS VC; close triangle: RHY B, BAS D or BAS DA, close diamond: RHY C; inverted open triangle: RHY M; star: RHY Z, open circle: BAS E; open square: BAS O; cross: UNC. (For interpretation of the references to colour in this figure legend, the reader is referred to the web version of this article.)

VC rocks follow the intermediate alteration trend (Fig. 3b).

4.2.2. Trace elements

The mafic volcanic rocks are characterized by relatively lower Al_2O_3/TiO_2, Zr/Al_2O_3, Th/Nb, La/Yb, Ga/Ti and Th/Zr than the felsic volcanic rocks (Fig. 4). The felsic volcanic rocks have been divided in several chemical groups based on specific immobile element plots, as mentioned before (Barrett, 2008, 2009; Barrett et al., 2008). RHY A is marked by its relatively higher Ga/Ti and Hf/Ti. RHY B is distinguished by its relatively higher Th/Nb. RHY C is characterized by its relatively lower Zr/Al_2O_3. RHY M is evidenced by its relatively lower Al_2O_3/TiO_2, Zr/TiO_2, Hf/Ti, Yb/La and Ga/Ti. RHY X shows relatively higher Zr/Al_2O_3 and Zr/Th. RHY Z is characterized by its relatively higher Al_2O_3/TiO_2, Nb/Zr and Ti/Ga (Fig. 4).

Using rock classifications with immobile elements, felsic rocks of chemotype RHY A, RHY B, RHY C, RHY X and RHY Z are classified as rhyodacite/dacite and rhyolite in Winchester and Floyd (1977) widely used graph (Fig. 3c) and as rhyolites using a recent classification

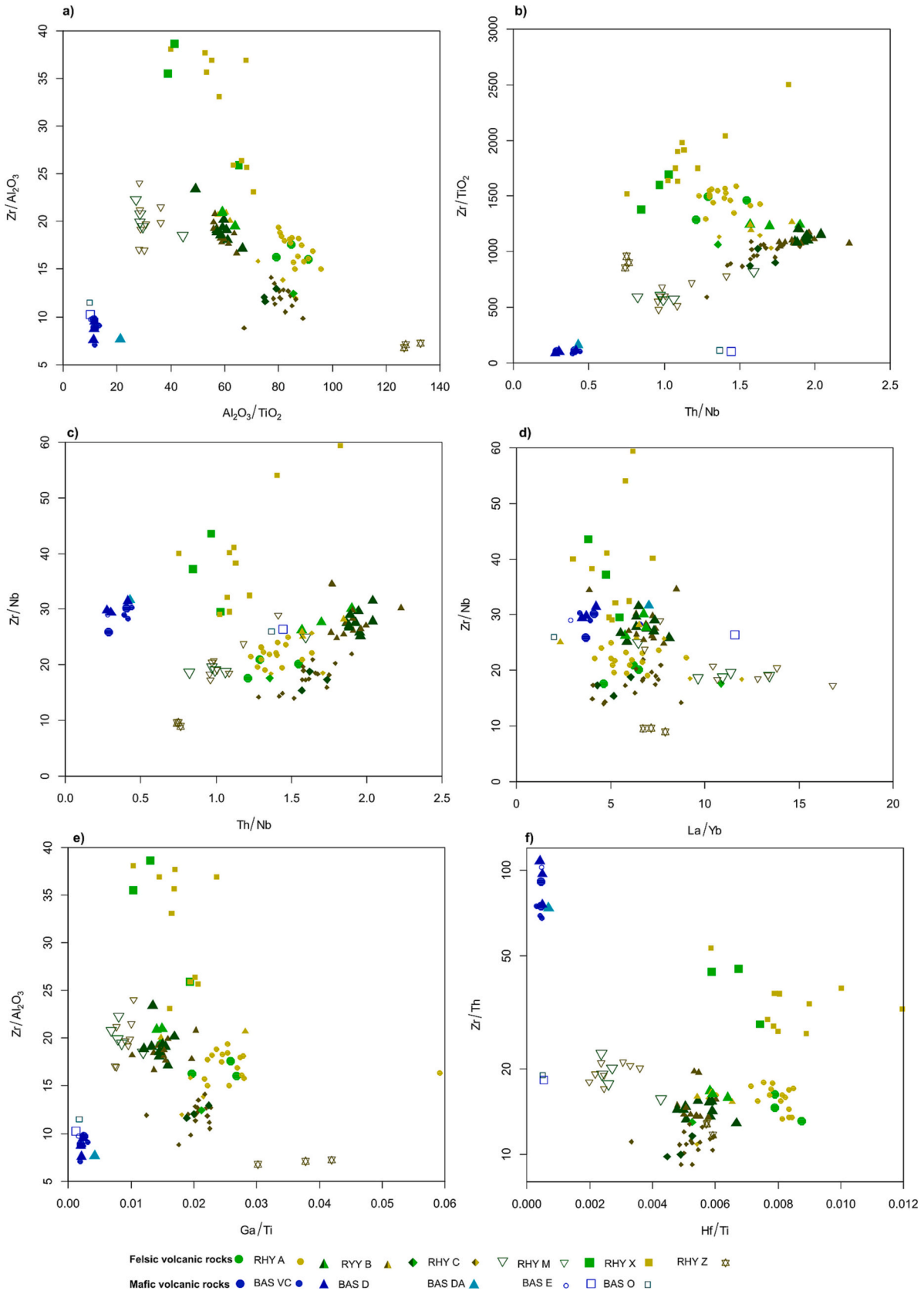

Fig. 4. Immobile element plots for the volcanic rocks of Aljustrel. a) Al_2O_3/TiO_2 vs. Zr/Al_2O_3; b) Th/Nb vs. Zr/TiO_2; c) Th/Nb vs Zr/Nb; d) La/Yb vs Zr/Nb; e) Ga/Ti vs. Zr/Al_2O_3 and f) Hf/Ti vs Zr/Th. Symbols as in Fig. 3.

scheme, based on machine learning, that uses 13 immobile elements (Lang et al., 2023). The felsic chemotype RHY X is classified as rhyodacite/dacite (Fig. 3c) or rhyolite/trachytic, respectively (see Table ST1). On the other hand, most mafic rocks in Fig. 3c plot in Andesite/Basalt field (except one sample, BAS DA, that plots in the Andesite filed). The machine learning method (Lang et al., 2023) classified the BAS D samples as basaltic andesite, the BAS DA sample as andesite, the BAS VC samples as basalt or basaltic andesite, the BAS O samples as basalts and the BAS E sample as andesite (see Table ST1).

Immobility of certain elements can be tested by plotting elements of interest against Zr or Nb (Cann, 1970; MacLean and Barrett, 1993), which was tested for each felsic chemotype proposed by Barrett (2008) and Barrett et al. (2008) (Figs. 3c–d; SF7). To remove slightly mineralized rocks, samples with Zn + Pb + Cu > 1000 or S > 1 % were not chosen for this geochemical study (Table ST1).

The high correlation coefficient (r > 0.80) for most of the REE, TiO_2, Al_2O_3, Th, Hf, Nb, Y and Ga of RHY B strongly support their immobility under the Aljustrel's hydrothermal system (Fig. SF7). For the other chemotypes, the correlation coefficients are poorer in comparison to RHY B. Chemotype RHY A shows good correlation between Nb or Zr with La, Nd, TiO_2, Al_2O_3, Th, Ta, Hf and Ga, whereas the higher correlation coefficients are higher with REE, TiO_2, Al_2O_3, Th and Hf and Ga for RHY C (Fig. SF7). The Megacrystal unit (RHY M) presents good correlation of Nb or Zr with LREE, most MREE, TiO_2, Ta and Ga (Fig. SF7). The chemotype RHY X has an overall strong correlation of the REE with Nb and a good correlation between Nb or Zr with TiO_2, Al_2O_3, Ta and Hf (Fig. SF7). Notably, Zr and Nb decoupling is observed in RHY M and RHY X, in which for the latter may represent heterogeneities of the group, as shown in Barrett's classification plot (Fig. 3d). Apart from RHY B and X, HREE show poor correlation degrees either with Nb or Zr (Fig. SF7).

4.3. Nd isotopes

The volcanism emplacement in Aljustrel took place between 353 and 359 Ma (Lains Amaral et al., 2021b), thus for the calculation of initial values and single- and two-stage model ages an age of 355 Ma was used (Table ST1). $\varepsilon Nd_{(355)}$ of the mafic rocks mostly range from +1.54 to +2.87, except for one BAS VC sample that presents a value of +5.48 (Fig. 5). For the felsic volcanic rocks, $\varepsilon Nd_{(355)}$ ranges from −5.07 to +0.54, except RHY X chemotype yielding systematically positive values (+0.98 to +1.79), slightly overlapping the values of the mafic volcanic rocks. Single-stage model ages (TDM) for felsic rocks varies between 1.1 and 1.6 Ga, except for one sample of RHY Z that yielded a value of 3.0 Ga. The two-stage model ages (2TDM) for this RHY Z sample yields a value of 1.4 Ga. Otherwise, TDM and 2TDM yielded more similar ages for each sample, with the latter yielding ~0.3 Ga younger ages than the former (Fig. 5). More radiogenic samples yield younger model ages (RHY X and one RHY B sample), and less radiogenic samples yield older model ages.

4.4. U-Pb in zircon

Five mafic volcanic samples were selected for zircon extraction, of which four (BAS E: GS18003_490; BAS VC: AS18005_491.5; BAS D: GS18003_231; GS18003_326) did not provide any zircon for analyses. The andesitic mafic sample (BAS DA: GS18003 318.4 m) provided 2 zircons (Appendix SA1), of which only one was concordant, yielding a single-grain Concordia age of 402.1 ± 15.5 Ma. Th/U ratio is 0.27, typical of felsic melts (Table ST2).

Sample ES16005_864 of chemotype RHY X yielded abundant zircon, and 15 were selected for analysis (Appendix SA1). The U—Pb data (Table ST2) yielded concordant analyses (Concordia distance, Vermeesch, 2021a, between −1.0 and 2.1 %, and all ellipses at 1σ intersect the Concordia, not shown), single-grain Concordia ages (Vermeesch, 2021a) between ~341 and ~387 Ma, and Th/U ratios between 0.56 and 1.27, which are typical of magmatic suites. However, the results show high common lead percentages (1.3–7.4 %), which may raise concerns about the uncertainty of the analyses. Indeed, $^{207}Pb/^{235}U$ errors are quite high (8 to 26 %).

For this work it is applied the IsoplotR's radial plot method (Vermeesch, 2021a, 2021b). After excluding the youngest age (~341 Ma) based on the age drop tail in the weighted average diagram (Fig. 6b) (Spencer et al., 2016; see also Lains Amaral et al., 2021b), the automatic

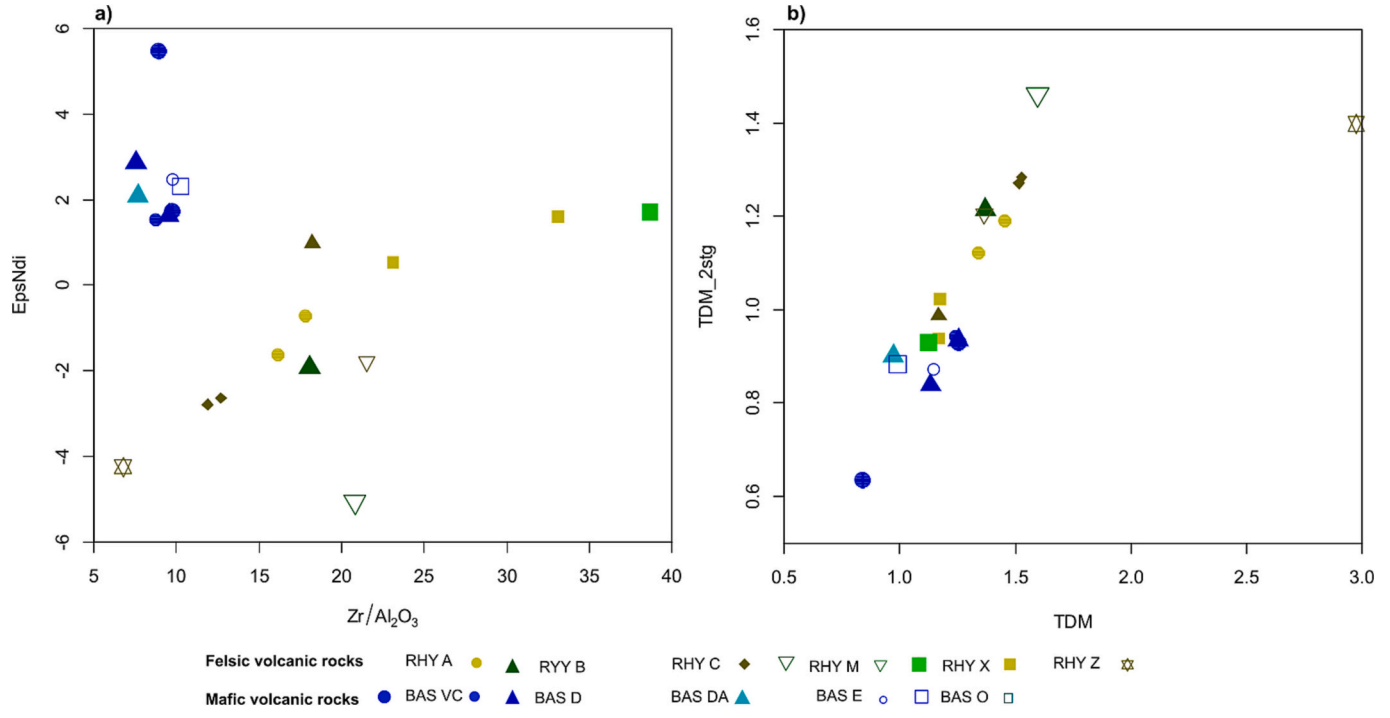

Fig. 5. Sm—Nd isotopic plots for the volcanic rocks of Aljustrel. a) Zr/Al_2O_3 vs. $\varepsilon Nd_{(355)}$; b) Nd-depleted mantle model ages (TDM) vs two stage model ages (TDM2).

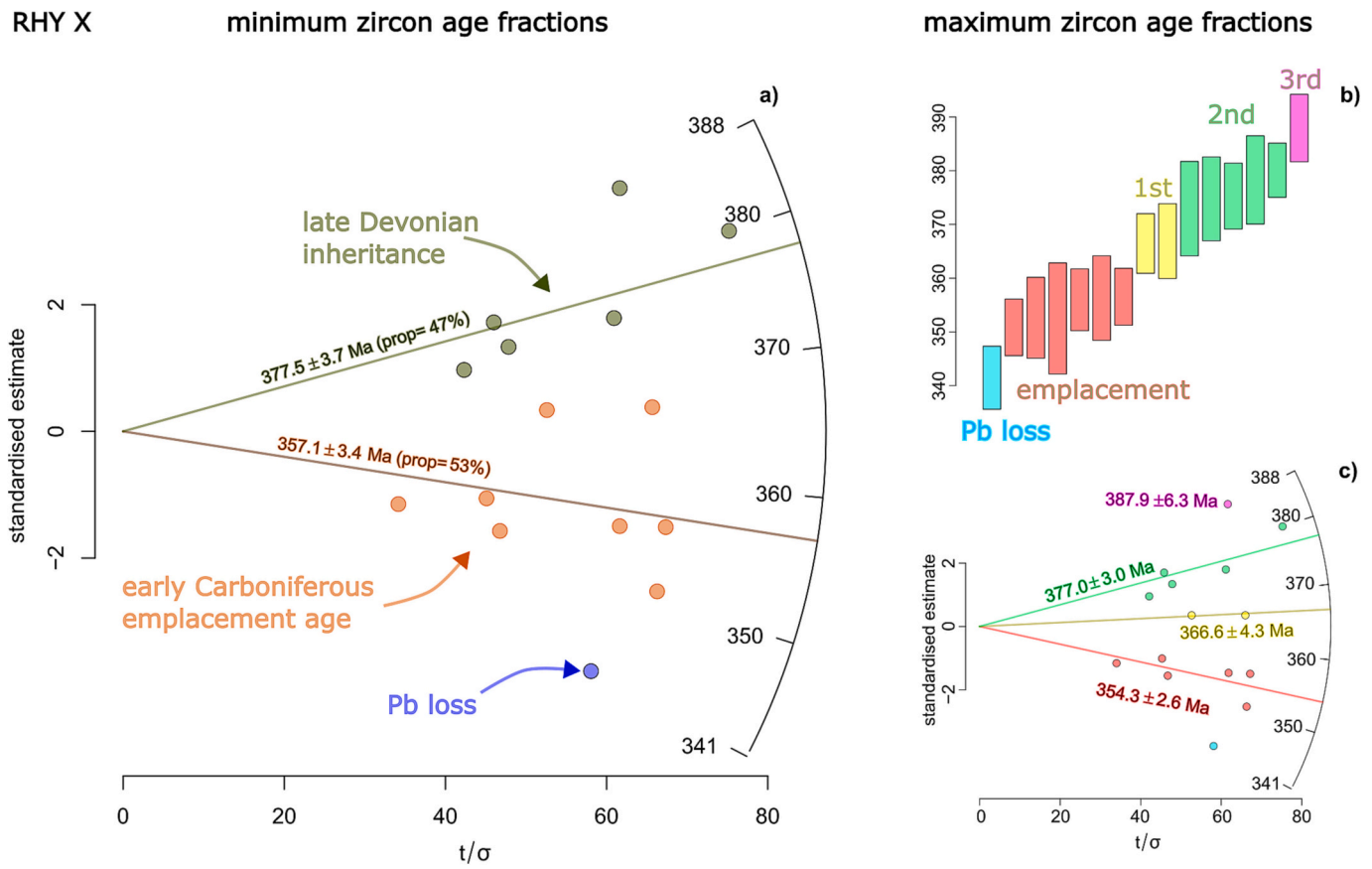

Fig. 6. U—Pb in zircon plots for the RHY X chemotype of Aljustrel (sample ES16005_864). a) Minimum zircon age fraction: automatic radial plot ages, yielding two populations (see text); b and c): maximum zircon age fractions: scattering of the radial plot and of the weighted average plot suggests four populations; radial plot ages calculated individually for each population. Pb loss analysis in blue (see text). (For interpretation of the references to colour in this figure legend, the reader is referred to the web version of this article.)

mode of the radial plot (Fig. 6a) yielded two age groups: 357.1 ± 3.4 Ma (n = 8; MSWD = 0.98), representing 53 % of the selected grains, and 377.5 ± 3.7 Ma (n = 6, MSWD = 1.50), representing the remaining 47 % of the selected grains, demonstrating the presence of a significant inherited population. Assuming the existence of several inherited ages (see Lains Amaral et al., 2021b), and careful visual inspection of the radial and weighted average plots, the RHY X may contain a maximum of 3 inherited ages (Fig. 6b–c). In this regard, the emplacement age of the sample would be 354.3 ± 2.6 Ma (n = 6, MSWD = 0.17), and the maximum inherited fractions for the RHY X would be 366.6 ± 4.3 Ma (n = 2, MSWD = 0.00), 377.1 ± 3.0 Ma (n = 5, MSWD = 0.10) and the single age of 387.9 ± 6.3 Ma.

5. Discussion

5.1. Classifying hydrothermal volcanic rocks

5.1.1. Felsic volcanic rocks

There are several schemes for the geochemical classification of felsic rocks (Barbarin, 1990; Bonin et al., 2020; Chappell and White, 1992; Eby, 1992; Frost et al., 2001; Frost and Frost, 2008; Hart et al., 2004; Irvine and Baragar, 1971; Lang et al., 2023; Le Bas et al., 1986; Leat et al., 1986; MacLean and Barrett, 1993; Maniar and Piccoli, 1989; Middlemost, 1994; Whalen et al., 1987; Winchester and Floyd, 1977). Rock classification (Winchester and Floyd, 1977), alkalinity (Leat et al., 1986) and ore-related classification schemes (Hart et al., 2004) are widely used in hydrothermal altered volcanic rocks, as ratios of the most immobile elements are applied (Fassbender et al., 2022; Piercey, 2010). On the other hand, alphabetic and multi-geochemical index classification schemes are mostly used in plutonic suites, involving major elements (Frost and Frost, 2008), petrographic associations (Chappell and White, 1992) or both (Bonin et al., 2020). In this regard, there are three main aspects to consider when it comes to classifying hydrothermally altered volcanic rocks. Firstly, there is no common ground classification for the extrusive and intrusive counterparts (Frost et al., 2016). Indeed, a recent review strongly suggests that granitoid chemistry and volcanic chemistry may not be either equivalent or complementary (Clemens et al., 2022). Secondly, chemical classification of felsic volcanic rocks should be independent of their petrogenesis, thus mantle-derived classification schemes must not be applied, as not all felsic volcanic rocks are derived from the evolution of mafic melts. Therefore, classifications based on the AFM (or their derivatives) (Irvine and Baragar, 1971; Ross and Bédard, 2009) are not considered. Furthermore, calc-alkaline and tholeiite evolved rocks overlap in the AFM diagram, as noticed by Irvine and Baragar (1971). Thirdly, classification schemes that use trace elements are rare, and even rarer for immobile elements. Indeed, a proper classification for hydrothermal altered volcanic rocks should be based on immobile element ratios, as these ratios are more probable to keep their original melt signatures (MacLean and Barrett, 1993). Accordingly, only a very few classification diagrams are applicable. Considering all the above, division between A-, I- and S-type (Whalen et al., 1987) and ore-related classification schemes (Hart et al., 2004) are adopted in this work.

The felsic volcanic rocks of Aljustrel are sub-alkaline (Fig. 3b), like most of the IPB felsic rocks (Quesada et al., 2019). They show typical Ga/Al ratios of A-type, as defined by Whalen et al. (1987) (Fig. 7a), and present Y/Nb ratios belonging to the subdivision A2-type (Eby, 1992) (Fig. 7b).

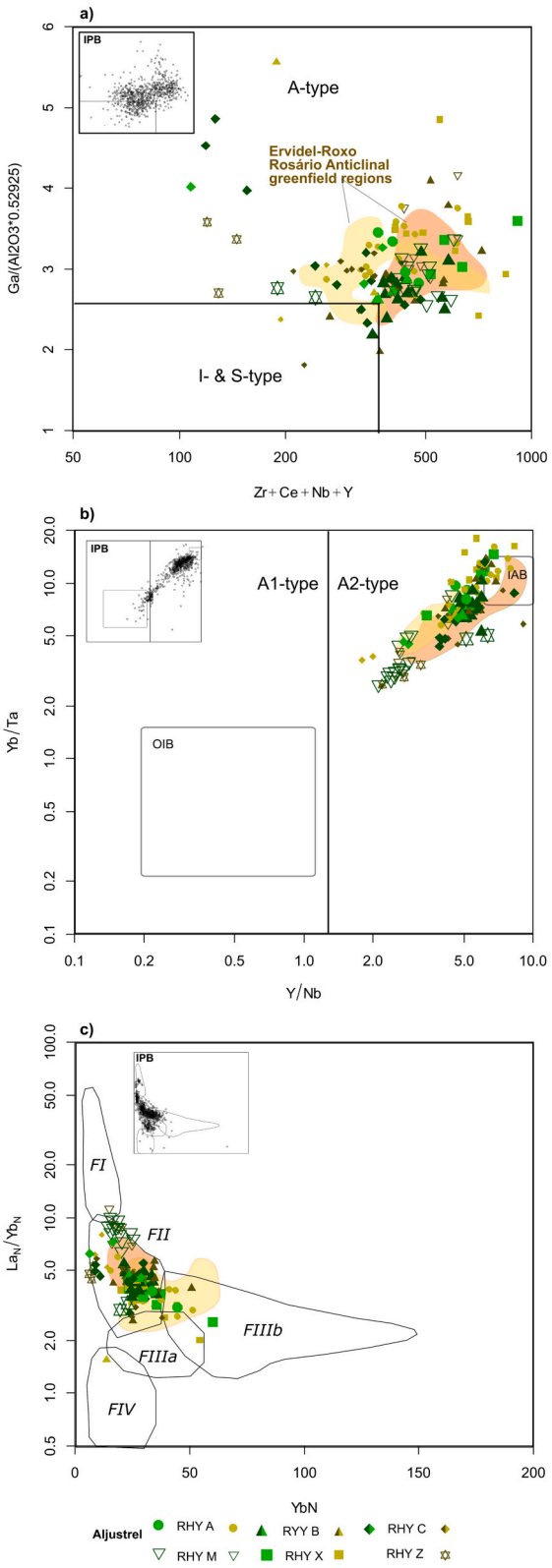

Fig. 7. Immobile elements classification for the felsic volcanic rocks of Aljustrel and, in smaller boxes, of the IPB (n = 860; personal database; Codeço et al., 2018; Gisbert et al., 2021; Pascual et al., 2021; Rosa, 2007; Rosa et al., 2006, 2004; Valenzuela et al., 2011a). Coloured areas correspond to felsic chemotypes from Ervidel-Roxo and Rosário anticlinal; a) Zr + Ce + Nb + Y vs Ga/Al (Whalen et al., 1987; modified by Ballouard et al., 2020); b) Y/Nb vs Yb/Ta (Eby, 1992); c) Yb_N vs La_N/Yb_N (Hart et al., 2004), normalized to Nakamura (1974). Symbols as in Fig. 3.

According to ore related classification (Hart et al., 2004), Aljustrel felsic rocks are classified as FII-type. According to Hart et al. (2004), FII-type rock can be associated to mineralized deposits, particularly those that were generated at depths of 10-15Km (upper crust - middle crust transition).

In other brownfield and greenfield regions of the IPB, the chemotypes of each region can also show Ga immobility under hydrothermal circulation as in Aljustrel. Thus, Ga/Al > 2.6 and Y/Nb > 1.2 of the great majority of the IPB felsic volcanic rocks (Fig. 7a–b) (e.g., Neves-Corvo, Rosário Anticline, Ervidel-Roxo, Águas Teñidas; Barrett, 2010; Codeço et al., 2018; Gisbert et al., 2021; Oliveira et al., 2013) and their melt inclusions (Marques et al., 2020) point out that A2-type magmatism was widespread in the IPB from the late Devonian, in the southern branch (e.g., Neves Corvo), to the early Carboniferous, in the northern branch (e.g., Águas Teñidas). In Phanerozoic times, A-type melts are more frequent in back-arc settings and post-collisional orogens (Condie et al., 2023), which has petrogenetic and geodynamic implications that will be addressed in the Section 5.2.5.

It should be mentioned that contrary to what is usually expected for A2-type rocks, the least altered rocks of the IPB plot systematically in the peraluminous and magnesian field (not shown). However, index-based classification schemes (Frost et al., 2001) are defined using major (mobile) elements and their meaning is difficult to assert and may produce biased results. Indeed, Barrett et al. (2008) has shown significant Mg, Fe, Al, Na, and Ca mass changes related to chloritization and sulphidation in the Aljustrel volcanic rocks, being the former also significant across the IPB (e.g., Codeço et al., 2018). Interestingly, the major elements of melt inclusions in quartz in the volcanic rocks of Figueirinha-Albernoa, Neves-Corvo and Serra Branca (Marques et al., 2020) also points to magnesian and peraluminous compositions. However, the abnormal Aluminous Saturation Index (ASI) values in the melt inclusion (ASI >2, not shown) points to some modification of the original melt, likely due to seawater interaction. In this regard, the magnesian and peraluminous character of the volcanic rocks of the IPB are likely meaningless.

Taking into to account the intrinsic issues regarding a proper classification for the hydrothermal volcanic rocks, in this work it is considered that the volcanic rocks of Aljustrel (as most other volcanic rocks of the IPB) are best classified as FII-A2-type sub-alkaline rhyolitic to dacitic volcanic suites.

5.1.2. *Mafic volcanic rocks*

Mitjavila et al. (1997) and Munhá (1983) identified tholeiite and alkaline basalts in the IPB. Conversely, these authors used mostly major elements to attribute the tholeiite affinity of the IPB sub-alkaline basalts. For the sub-alkaline mafic rocks of Aljustrel and other areas of the IPB (e.g., El Almendro–Villanueva de los Castillejos and Aguas Teñidas) major element-based classification is ambiguous. They plot in the tholeiitic field of the FeOt/MgO-SiO_2 diagram (Miyashiro, 1974; not shown). However, in the AFM (Irvine and Baragar, 1971; not shown) and ATM (Vermeesch and Pease, 2021; not shown) diagrams, these sub-alkaline basalts plot in the calc-alkaline field. Nonetheless, these diagrams use mobile elements such SiO_2 and Total Alkalis and, as a rule of thumb, the present work solely considers immobile trace element ratios.

The mafic volcanic rocks of Aljustrel have sub-alkaline affinity (Fig. 3), plot in the volcanic arc array (Pearce, 2008) (Fig. 8b) and in the calc-alkaline or "transitional" fields (Cabanis and Lecolle, 1989; Ross and Bédard, 2009) (Fig. 8a,c), and have Th/Yb > ~0.3 and Ce/Yb > 5 ratios, which are considered of calc-alkaline affinity (Pearce, 1982). Furthermore, they have Ti/V ratios (30-50) higher than tholeiitic arc rocks (i.e., Ti/V > 20), which are typical of calc-alkaline suites (Shervais, 2022). Conversely, some of the mafic rocks that are classified as "transitional" in Fig. 8c have $2 < (La/Nb)_N^{PM} < 3$, whereas others classified as calc-alkaline in Fig. 8c have $1.5 < (La/Nb)_N^{PM} < 2$. For comparison, mafic volcanic rocks from other IPB areas were plotted together with Aljustrel samples on the immobile diagrams (Fig. 8). The El

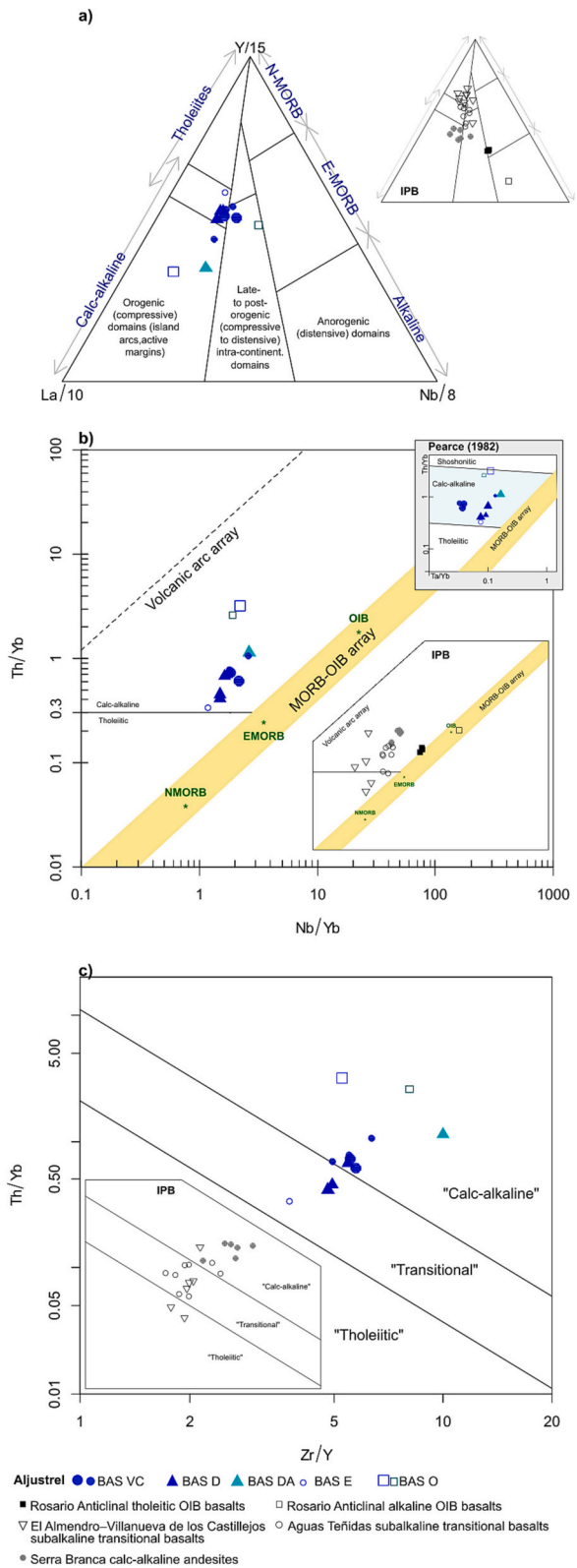

Fig. 8. Immobile elements classification plots for the mafic volcanic rocks of Aljustrel, and, in smaller boxes, of the alkaline Rosário Anticlinal lavas, selected subalkaline El Almendro–Villanueva de los Castillejos lavas, subalkaline Aguas Teñidas lavas and intermediate Serra Branca lavas (Gisbert et al., 2021; Oliveira et al., 2013; Pascual et al., 2021; Rosa et al., 2006) a) La/10-Y/15-Nb/8 (Cabanis and Lecolle, 1989). b) Nb/Yb vs Th/Yb (Pearce, 2008). c) Zr/Y vs Th/Nb (Ross and Bédard, 2009). Symbols as in Fig. 3.

Almendro–Villanueva de los Castillejos (Pascual et al., 2021) and Aguas Teñidas (Gisbert et al., 2021) mafic rocks have some similarities with the mafic volcanic rocks of Aljustrel. They plot in the Andesite/Basalt field and have sub-alkaline affinity (Nb/Y < 0.67, Winchester and Floyd, 1977). In addition, they plot in the volcanic arc array (Fig. 8b) and have calc-alkaline affinity in the Pearce (1982) classification diagram (not shown). In the Zr/Y-Th/Nb diagram most rocks are classified as transitional (Fig. 8c). However, El Almendro–Villanueva de los Castillejos plot in the tholeiitic field in the La/10-Y/15-Nb/8 diagram (Fig. 8a), but have $(La/Nb)_N^{PM} > 2$. This suggests that the degree of Nb anomaly is independent of its geochemical affinity. Thus, the sub-alkaline mafic rocks selected in this work, including Aljustrel, show a geochemical fingerprint that ranges between tholeiitic to calc-alkaline affinities. Nonetheless, overall, the mafic volcanic rocks of Aljustrel show a closer affinity to calc-alkaline. Undisputed calc-alkaline affinity has only been described in the intermediate mafic volcanic rocks (e.g., Serra Branca; Rosa et al., 2006) (Fig. 8).

In contrast to the sub-alkaline affinity of mafic rocks of the IPB, minor alkaline basalts (Nb/Y > 0.67, Winchester and Floyd, 1977) have also been identified (Mitjavila et al., 1997; Munhá, 1983; Oliveira et al., 2013; Rosa et al., 2004). These have been found in the Rosário Anticline (Oliveira et al., 2013), plotting in the MORB-OIB array (Fig. 8b), being classified as OIB tholeiitic basalts or OIB alkaline basalts in the Nb/Yb-TiO_2/Yb diagram (not shown) (Pearce, 2008). The OIB affinity is also depicted by their common high Ti/V ratios (>43; Shervais, 2022).

Considering these observations, the mafic volcanic rocks of Aljustrel are regarded as having calc-alkaline affinity, similar to the basalts of Aguas Teñidas, and in between the calc-alkaline andesites of Serra Branca and the more tholeiitic basalts of El Almendro–Villanueva de los Castillejos, clearly contrasting with the OIB basalts of the Rosário Anticline.

5.2. *Assessing the role of the continental crust*

5.2.1. *Mantle magmatism and crustal contamination*

The mantle is composed of distinctive isotopic reservoirs as attested by primitive basic magmatism. Primitive MOR basalts record a highly Nd radiogenic isotopic source (i.e., ~+ 10), the depleted mantle, whereas intermediate Nd isotopic signatures (i.e., ~+5), PREMA and HIMU, are often recorded in primitive OIB and arc-related basalts. Less Nd radiogenic sources (i.e., ~ −5) of primitive arc-related basalts, EM1 and EM2, are attributed to subduction-related metasomatism (Zindler and Hart, 1986). On the other hand, mantle-derived magmas may modify their composition through the interaction with the Nd unradiogenic (i.e., ~−15) continental crust (or their partial melting products) (De Campos et al., 2011; DePaolo and Wasserburg, 1979). In this regard, the slightly depleted signature of most mafic rocks of Aljustrel, $\varepsilon Nd_{(355)}$ from +1.54 to +2.87 (Fig. 5a) may indicate a depleted mantle source affected by subduction-related metasomatism, a PREMA source or continental crust contamination. However, one mafic sample, classified as basalt (Lang et al., 2023) (Table ST1), yielded a high Nd radiogenic signature, $\varepsilon Nd_{(355)} = +5.48$, the highest value so far registered in the IPB, more radiogenic than the radiogenic alkaline basalt (FP-40) (Mitjavila et al., 1997) with $\varepsilon Nd_{(350)} = +3.62$, which has a positive Nb anomaly (Fig. 9a). This suggests that the orogenic signature of the Aljustrel samples, Nb-Ta-Ti negative anomalies and Th positive anomaly is related to the mantle source (Fig. 9) and not related to crustal contamination, which is corroborated by the lack of zircons in the heavy concentrates (see Section 4.4). Furthermore, this sample falls in the OIB-fertile mantle array (Fig. 10a). Thus, the orogenic signature and calc-alkaline affinity of the Aljustrel mafic rocks can be envisaged as a primary feature attributed to the mantle source. This is in agreement with Munhá (1983), which suggested the involvement of two mantles sources to explain the geochemical variability of the mafic rocks in the IPB: an enriched subduction-related source, such as the Aljustrel calc-alkaline rocks, and a depleted source, such as the OIB-like rocks of the Rosário

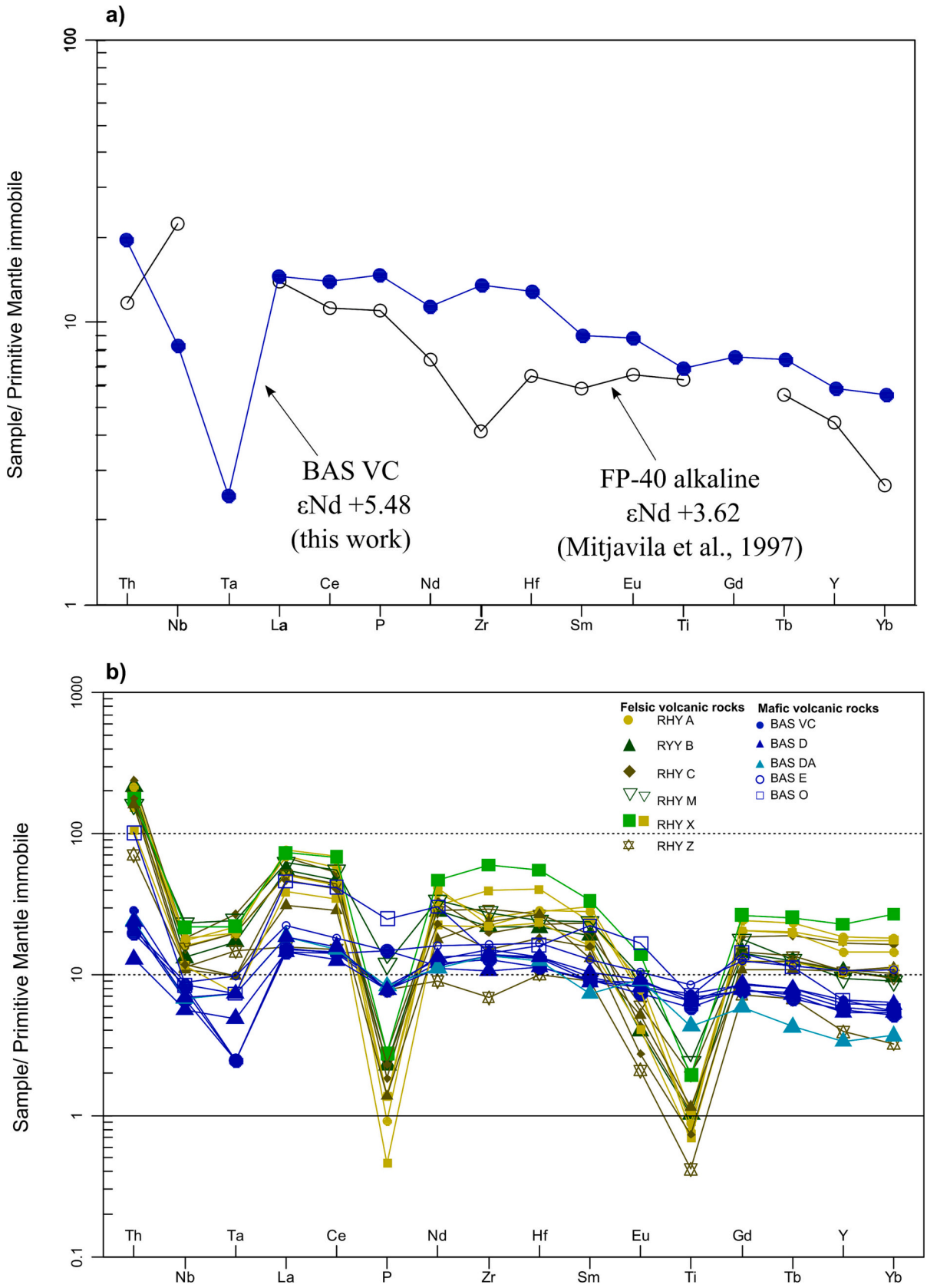

Fig. 9. Primitive mantle-normalized incompatible-immobile element diagram. a) Comparison between the most radiogenic calc-alkaline mafic rocks of Aljustrel (BAS VC) and the alkaline radiogenic mafic sample from Mitjavila et al. (1997) (FP-40). b) mafic and felsic volcanic rocks from this study with Sm—Nd analyses. c) Symbols as in Fig. 5. Normalization after Sun and McDonough (1989).

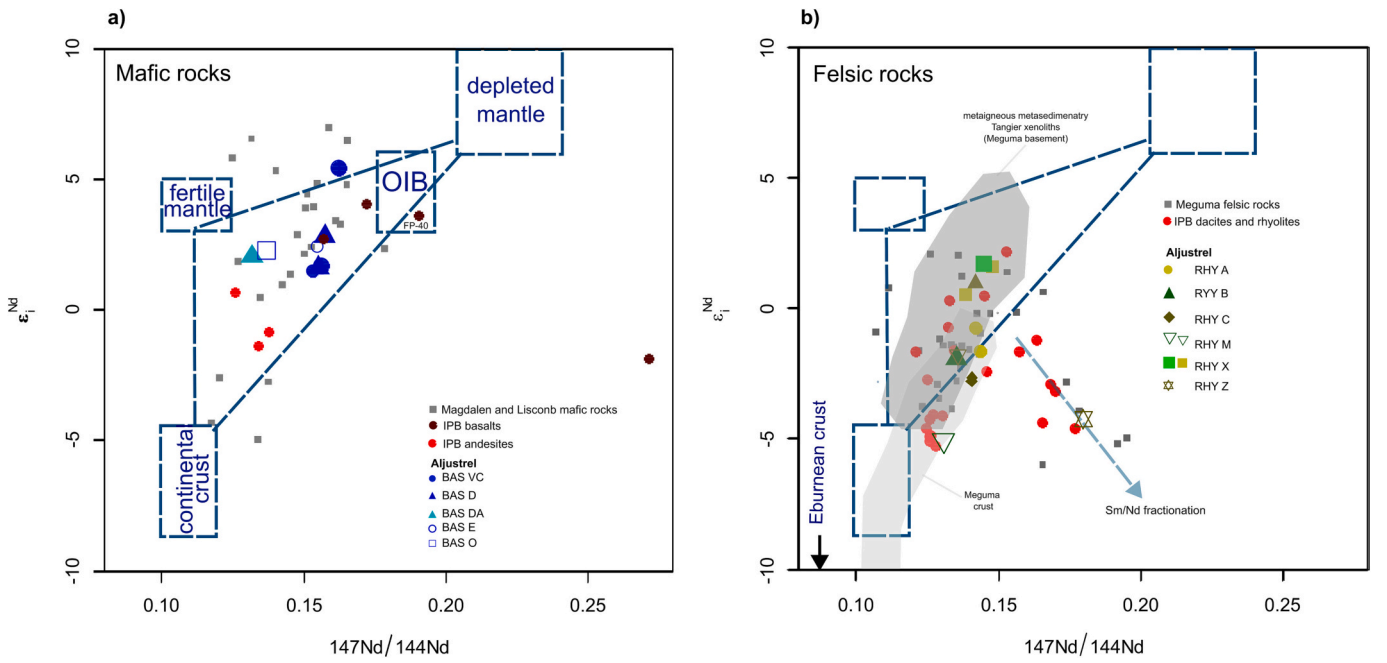

Fig. 10. $^{147}Nd/^{144}Nd$ vs εNd_i for a) mafic and b) felsic volcanic rocks of Aljustrel, IPB (Donaire et al., 2020a; Mitjavila et al., 1997; Pascual et al., 2021; Valenzuela et al., 2011b), Meguma Upper Devonian-Early Carboniferous mafic rocks of Liscob and Magdalen (Clarke et al., 1993; Pe-Piper and Piper, 1998), Meguma xenoliths of Tangier (Eberz et al., 1991). Meguma Cambrian-Ordovician crust (Waldron et al., 2009). Arrow indicates samples with high discrepancy between TDM and 2TDM ages (>0.5 Ga) that might indicate Sm—Nd fractionation during partial melting (Bea et al., 2023).

Anticline or sample FP-40 (Figs. 8, 10). In addition, $(Tb/Yb)_N^{PM}$ values below 1.8 of Aljustrel volcanic rocks (1.07 to 1.41) and IPB sub-alkaline and OIB tholeiitic basalts (~1 to ~1.6) (Gisbert et al., 2021; Oliveira et al., 2013; Pascual et al., 2021) suggests a spinel-lherzolite, garnet-free, mantle source (see Wang et al., 2002). In contrast, the OIB alkaline basalt of the Rosário Anticlinal has a ratio $(Tb/Yb)_N^{PM}$ of ~2.1 suggesting that partial melting occurred at deeper sections of the mantle, where garnet is stable.

In Fig. 10a, the IPB alkaline sample FP-40 (Mitjavila et al., 1997) falls in the OIB field, suggesting the rather primary feature of this sample (Mitjavila et al., 1997). On the other hand, the more radiogenic sample retrieved in hole PM15001 falls between the fertile mantle and OIB fields, which could suggest some degree of mixing between them, e.g., modified subduction-related metasomatized source by asthenospheric upwelling or magma mixing with OIB basalts.

The other less radiogenic Aljustrel and the IPB mafic rocks require a three-component partial melting and mixing between depleted and enriched sources and a crustal contaminant (Fig. 10a) (see also Pollock et al., 2015). From Fig. 10a, the crustal contaminant in the IPB andesites was likely significant. Indeed, Mitjavila et al. (1997) suggested that andesites may have formed by assimilation of crustal materials (see also Rosa et al., 2004). Other distinctive features between andesite and other mafic rocks of the IPB have been established. The IPB intermediate rocks have negative Eu anomalies and basalts show near flat Eu/Eu*. In addition, the IPB andesites have more pronounced REE fractionation than the IPB basalts (Mitjavila et al., 1997; Munhá, 1983). Indeed, the andesites of Serra Branca have moderate negative to near-flat Eu negative anomalies (Eu/Eu* = 0.5–0.9; Rosa et al., 2006) and $(La/Yb)_N^C$ = 3.08-6.80, whereas basalts from El Almendro–Villanueva de los Castillejos (Eu/Eu* = 0.86–1.12; $(La/Yb)_N^C$ = 1.16–2.60) and Aguas Teñidas (Eu/Eu* = 0.74–1.08; $(La/Yb)_N^C$ = 2.01–2.79) show near-flat, slightly negative to slightly positive, Eu anomalies and lower LREE/HREE fractionation. In Aljustrel, most mafic rock have near-flat Eu anomalies (Eu/Eu* = 0.82–1.19) and moderate REE fractionation $(La/Yb)_N^C$ = 1.33–2.81, but two more hydrothermal altered BAS VC rocks show moderate Eu negative anomalies (Eu/Eu* = 0.53–0.56) and slightly more pronounced REE patterns ($(La/Yb)_N^C$ = 2.61–4.38) suggesting that they might represent more evolved composition (see also Fig. 3b). Interestingly, andesite BAS DA has a moderate positive anomaly (Eu/Eu* = 1.39, Fig. 9b), which is unusual for the andesitic rocks of the IPB, precluding its origin by fractional crystallization of plagioclase from basaltic melts or significant contamination by crustal material. However, it does not exclude fractional crystallization dominated by olivine and pyroxene.

5.2.2. *Source and origin of the A2 type magmatism*

It has long been established that the felsic rocks of the IPB did not derive from basaltic magmas through AFC processes (Mitjavila et al., 1997; Munhá, 1983). This is corroborated by the different mafic and felsic trends on immobile element ratios, such as Zr/Nb versus $\varepsilon Nd_{(355)}$ (Fig. 11a) and REE fractionation patterns (Figs. 9b and 11b–c). In addition, the felsic rocks have a great proportion of inherited zircons (Lains Amaral et al., 2021b), implying a significant role of crustal material in their genesis (see discussion in Section 5.2.4).

The felsic volcanic rocks of Aljustrel are characterized by weak to moderate LREE/HREE ($(La/Yb)_N^C$ ~ 2.5–7) and LREE/MREE ($(La/Sm)_N^C$ ~ 2–3) fractionation, and near flat MREE/HREE to weak fractionation ($(Gd/Yb)_N^C$ ~ 0.9–2.5) (Fig. 11d–f). These have a negative correlation to $\varepsilon Nd_{(355)}$, with the most juvenile rhyolite (RHY X) yielding less fractionated REE patterns, more similar to the moderately radiogenic mafic rocks (Fig. 11d–f). The flat HREE pattern suggests a garnet-free source (Fig. 11b). In addition, according to Hart et al. (2004), the LREE fractionation typical of FII-type rocks (Fig. 7c) suggests an amphibole-plagioclase bearing source. This is in agreement to the view that A2-type melts may have derived from hydrous mineral-bearing sources (Gao et al., 2016; Patiño Douce, 1997). In addition, the negative Eu/Eu* anomalies (Fig. 11c), which has been related to feldspar-bearing sources in the IPB (Donaire et al., 2020a), may explain the high Ga/Al ratios of the Aljustrel A2-type rocks, as Ga is favorably excluded from the An-rich plagioclase relatively to Al (Collins et al., 1982 and references therein). Considering the possibility of magma mixing between mantle- and crustal-derived melts, which have been also described in A2-rocks

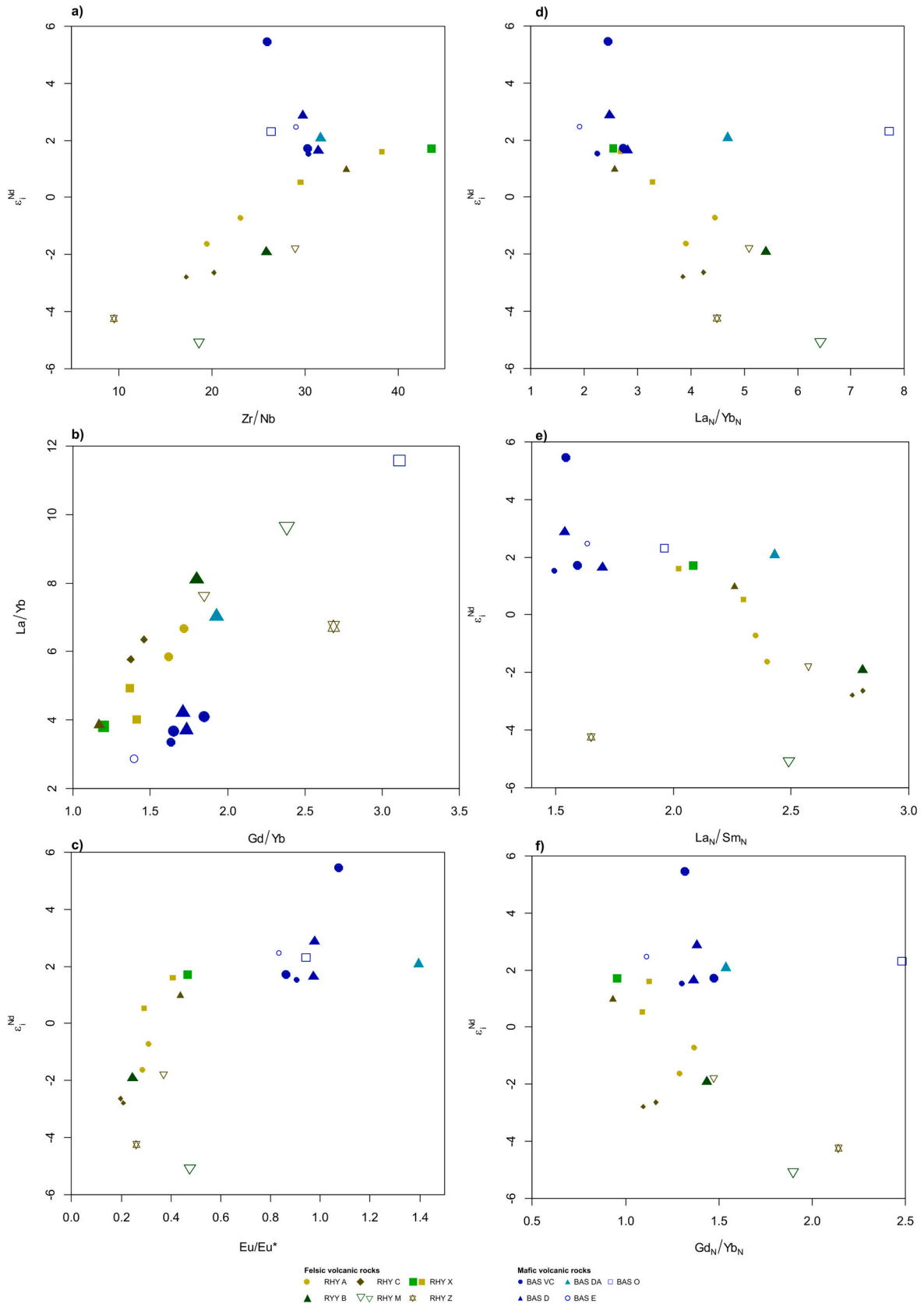

Fig. 11. Immobile elements ratio plots for the volcanic rocks of Aljustrel Sm-Nd analyses. a) Zr/Nb vs $\varepsilon Nd_{(355)}$; b) Gd/Yb vs La/Yb; c) Eu/Eu* vs Zr/Nb vs $\varepsilon Nd_{(355)}$; d) $(La/Yb)_N$ vs $\varepsilon Nd_{(355)}$; e) $(La/Sm)_N$ vs $\varepsilon Nd_{(355)}$; and; f) Symbols as in Fig. 5. Normalization after Nakamura (1974). Symbols as in Fig. 5.

(Bonin, 2007; Kerr and Fryer, 1993; Wang et al., 2019; Yang et al., 2006), the higher Ga/Al ratios of the felsic rocks relatively to the mafic rocks coupled with the Eu negative anomaly of the former reinforces that the A2-type signature of Aljustrel felsic rocks must be related to intracrustal partial melting.

5.2.3. Significance of model ages: Avalonian (s.l.) crust and magma mixing

Model ages of igneous rocks are useful to estimate the residence time from which a given crustal material was extracted from the mantle (Bea et al., 2023). In this regard, model ages of mantle-derived melts have little significance (Eberz et al., 1991). For crustal-derived melts, model ages are indicators of the (average) age of the source. As pointed out by Bea et al. (2023) two-step model age calculations (2TDM) are least affected by Sm/Nd fractionation during partial melting, and thus, are adopted in this work (see also Fig. 10a). The 2TDM of the felsic volcanic rocks of Aljustrel varies between 0.93 and 1.46 Ga (Fig. 5b). These ages are younger than the 2TDMs of the Tournaisian sedimentary cover of Aljustrel (1.36–1.74 Ga, Luz et al., 2022) and of the Middle Devonian-Visean sedimentary cover of the Iberian Pyrite Belt (1.36–1.90 Ga, Luz et al., 2022) (Fig. 12a,c). Indeed, this feature, similar to the TDM found in Nova Scotia, has been used as an argument favoring an affinity of the IPB to the Meguma Terrane (Braid et al., 2011). Recently, zircon detrital age patterns of the oldest known rocks of the IPB have also been related to Meguma Terrane (Lains Amaral et al., 2022b). In addition, whole rock Sm—Nd of the volcanic rocks of the IPB and Hf isotopes in zircon are also similar to those reported for the Devonian-Carboniferous igneous rocks of Meguma Terrane (Fig. 10) (de la Rosa et al., 2002). Thus, considering a Meguma affinity for the IPB, the metasedimentary and meta-igneous xenoliths retrieved in the Late Devonian Tangier dike system (Dostal et al., 2006) are crucial to understand the nature of the crust beneath Meguma Terrane (Eberz et al., 1991; Shellnutt and Dostal, 2022). It has been suggested that the ~1.0 Ga Sm—Nd model ages and minor occurrence of Mesoproterozoic zircons in the metasedimentary xenoliths are indicative of an Avalonian crust beneath the Meguma Terrane as a result of thrusting of Meguma over Avalonia during their amalgamation in the Devonian (Eberz et al., 1991; Shellnutt et al., 2019). On the other hand, zircons retrieved from the mafic xenoliths have the so-called “West African Craton signature” and lack Mesoproterozoic zircons, suggesting that unknown middle and/or lower crust of Meguma Terrane was deprived of Mesoproterozoic rocks, and composed of Neoproterozoic and Paleoproterozoic rocks (Shellnutt and Dostal, 2022). The felsic volcanic rocks of the IPB fall in the field of the metasedimentary and meta-igneous xenoliths of Tangier (Fig. 10b), so melting of a crust similar to these xenoliths could explain the isotopic variability of the felsic rocks of the IPB. Taken together, the late Neoproterozoic-middle Mesoproterozoic 2TDM of the felsic rocks of the IPB (Fig. 12a,d) (0.89–1.46 Ga; this work; Donaire et al., 2020a; Mitjavila et al., 1997; Pascual et al., 2021; Valenzuela et al., 2011a, 2011b) might be interpreted as a result of: i) melting Avalonian crust (TDM = 1.0–1.2 Ga; Murphy and Nance, 2002) followed by contamination by Meguma crust (2TDM = 1.20–2.21 Ga; Barr et al., 2022), considering a continental crust composed of Avalonia below Meguma; ii) melting of both Cadomian juvenile rocks and Eburnean-derived crust, considering a West African-type basement; iii) melting of igneous rocks crystallized from melts as referred in previous point; and iv) melting Proterozoic felsic crustal rocks and Devonian mafic igneous rocks (see Lains Amaral et al., 2021b). These sources are in agreement with the negative correlation between REE fractionation and $\varepsilon Nd_{(355)}$ (and model ages) (Fig. 11d–f) and positive correlation between Eu/Eu* and $\varepsilon Nd_{(355)}$ (Fig. 11c). Indeed, crustal contamination of Avalonian-derived magmas by Meguma crust; or relative increment of the Eburnean felsic crust relatively to the more juvenile crust would tend to increase REE fractionation and model ages and decrease $\varepsilon Nd_{(355)}$ and Eu/Eu* anomalies. As such, the variable model ages of the Aljustrel and other IPB zircons (Fig. 12) and volcanic rocks suggest that the Eburnean crust may have (indirectly) took part of their genesis.

A previous Lu—Hf in zircon study in the IPB (Rosa et al., 2009) shows a significant variation of εHf_i (−15 to +8). Disequilibrium melting has been claimed to cause the high variability Lu—Hf in some felsic rocks, as Hf is mainly controlled by zircon melting. Experimental studies concluded that partial melting and partial dissolution of zircon would generate melts with higher Lu/Hf and more radiogenic Hf than the source (Wang et al., 2018). In addition, isotopic variability of the partial or total dissolved zircon could be “transferred” to the autocryst or crystal overgrowth due to Zr slow diffusion in felsic melts (Farina et al., 2014). Thus, considering the significant inherited zircon population found in the Aljustrel volcanic rocks, the Hf isotopic variability could have resulted from different degrees of partial melting, where the zircons with quite high εHf_i (+8) represent melts generated by low degrees of partial melting (i.e., low zircon dissolution efficiency) or have been acquired from the zircons of the protolith(s). The strong correspondence between Sm—Nd whole-rock and Lu—Hf in zircon 2TDM model ages (~1.3 Ga) at Aljustrel (Fig. 12a,b), but also at IPB (~1.2 Ga; Fig. 12d,e), strongly suggests that Hf isotopic variability is not a result of disequilibrium melting. Furthermore, it also suggests that the petrogenetic process that gave rise to the observed Hf isotopic variability in zircon is also responsible for the Sm—Nd isotopic range of the whole-rock in the felsic volcanic rocks of Aljustrel and the IPB. Although the above crustal-dominated model(s) can explain the observed isotopic signatures of the Aljustrel and IPB felsic volcanic rocks and Lu—Hf signatures in zircon autocrysts (i.e., inherited from previous zircons), magma mixing has also been proposed to account for the high isotopic variability in felsic rocks (Griffin et al., 2002). Furthermore, magma mixing has been recently suggested to be an important mechanism in the IPB (Marques et al., 2020) and coupling between Hf and Nd model ages, indeed, favors such model. In this regard, strongly juvenile (up to $\varepsilon Hf_i = +7.94$) and unradiogenic Hf (down to $\varepsilon Hf_i = -15.28$) zircon autocrysts of Aljustrel and variable εNd_i (−5.07 to +1.79) may indicate the involvement of metasedimentary and juvenile melts. Thus, the volcanic rocks of IPB could have originated by magma mixing between juvenile mantle melts and isotopic variable crustal-derived melts. This process seems to explain the intermediate compositions and the high contents of V and V/Y, up to 188 ppm and 31.4, respectively, in the Albernoa melt inclusions of felsic rocks (Marques et al., 2020). However, in Aljustrel, the chemotype with the highest vanadium content (V = 36–57 ppm, V/Y = 0.8–1.2, V/Sc = 3.25–5.4), RHY M, contains the most unradiogenic sample with a value $\varepsilon Nd_{(355)}$ of −5.07, whereas the more juvenile chemotype, RHY X, has lower values of vanadium (V = 5–18 ppm, V/Y = 0.03–0.5, V/Sc = 0.28–2.25). This implies that the slight radiogenic signatures of RHY X cannot have been derived from mafic melts. In this scenario, model ages of the Aljustrel felsic rocks represent source heterogeneities, in which the more unradiogenic signatures point to crustal sources as old as 3.23 Ga for Lu—Hf isotopes (Fig. 12b) and 1.47 Ga for Sm—Nd isotopes (Fig. 12d), unfolding a long-time crustal residence source, such as the West African basement. Taken together, two main petrogenetic processes can be envisaged for the chemical variability of the volcanic rocks of IPB: i) mantle-derived basic melts variably affected by crustal material (with felsic melt mixing or upper crust assimilation), generally characterized by high values of vanadium (such as in e.g., Albernoa samples); and ii) felsic-derived melts, that likely have not mixed with mafic melts and were barely affected by country rocks, generally characterized by much lower values of vanadium (such as in e.g., Aljustrel samples).

5.2.4. Zircon inheritance and crustal recycling

U—Pb zircon age spectrum can also be useful in assessing the nature of the continental crust. The felsic volcanic rocks of Aljustrel are characterized by a significant antecryst zircon population (i.e., 40–50 Ma continuous zircon populations preceding the emplacement zircon population; Lains Amaral et al., 2021b). In Rosário Anticline, including Neves-Corvo mine, similar inherited zircons have also been identified (Oliveira et al., 2013; Pereira et al., 2021; Solá et al., 2015). These

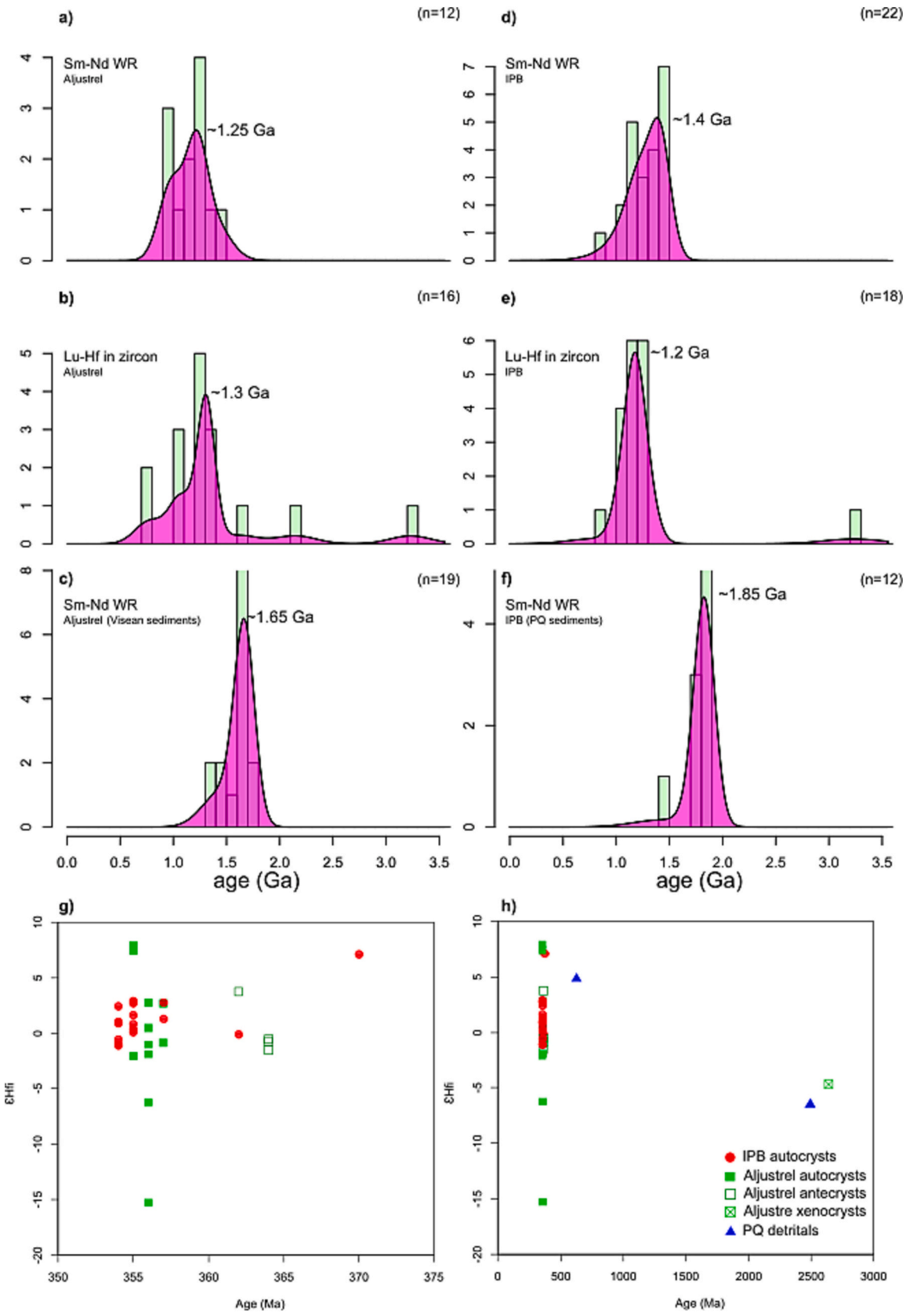

Fig. 12. KDE for two-stage model ages of Sm—Nd (whole-rock) in a) Aljustrel felsic rocks (this study), d) other volcanic rocks in the IPB (Donaire et al., 2020a; Mitjavila et al., 1997; Pascual et al., 2021; Valenzuela et al., 2011b) c) Aljustrel sediments (Luz et al., 2022) and f) IPB PQ sediments (Luz et al., 2022). KDE for two-stage model ages Lu—Hf (in zircon) in b) Aljustrel and e) other volcanic rocks in the IPB (Rosa et al., 2009). g–h) zircon U—Pb age vs zircon ƐHfi of Aljustrel and the IPB. Note that the early zircon ages identified by Rosa et al. (2009) are reinterpreted as antecryts (see Lains Amaral et al., 2021b).

antecrysts must be related to recent igneous activity and not to sedimentary contributions, as the latter would provide large proportions of pre-Phanerozoic zircons, namely Cadomian-Pan-African fractions (see e.g. Braid et al., 2012), which is not the case as only a tiny fraction of the analyzed zircons in the volcanic rocks of the IPB yield pre-Phanerozoic ages (Lains Amaral et al., 2021b).

Thus, antecrysts can be envisaged as a direct result of previous igneous rocks, such as plutons, dykes, or other melt form entrapped in the crust, pointing to protractive melting scenarios, such as prolonged crystal mushes, MASH (melting–assimilation–storage–hybridization) zones and or successive remelting of zircon-bearing rocks (Annen et al., 2006; Bindeman and Simakin, 2014; Jackson et al., 2018). Indeed, it has been suggested that a lower crustal hot zone (heated by mafic underplating) may be suitable for segregation and incubation of melts for extended periods (up to >30 Ma), producing zircons that latter can be incorporated in the melts that ascend to middle and upper crustal levels (Archibald et al., 2021; Bickerton et al., 2022; Hoseong et al., 2024; Miles and Woodcock, 2018). Nonetheless, in such conditions, partial remelting of igneous intrusions (pluton or dykes) is also possible (Hildreth and Moorbath, 1988), which is consistent with zircon inheritance in felsic magmas as deriving mostly from the source (Bea et al., 2021). This would require that, at depth, magmas with high water contents were being formed by the breakdown of hydrous minerals (e.g.: amphibole) at the source and exsolving water from underplated mafic intrusions. In addition, mantle-derived magma underplating induces an increase in heat flux that allows larger and faster melt extraction rates, which prevents the melt from reaching Zr sub-saturation, thus reducing dissolution of the zircons incorporated from the source (Bea et al., 2021). A felsic MASH, developed at the middle crust, might have also the proper ingredients to provide water-rich melts and fast rates of melt extraction. Indeed, granitoid intrusions may provide heat to the crust inducing fast enough melting and exsolving water into the crust, producing water-rich magmas (Schwindinger and Weinberg, 2017). Fast extraction rates, in mafic or felsic MASH zones, would prevent isotopic

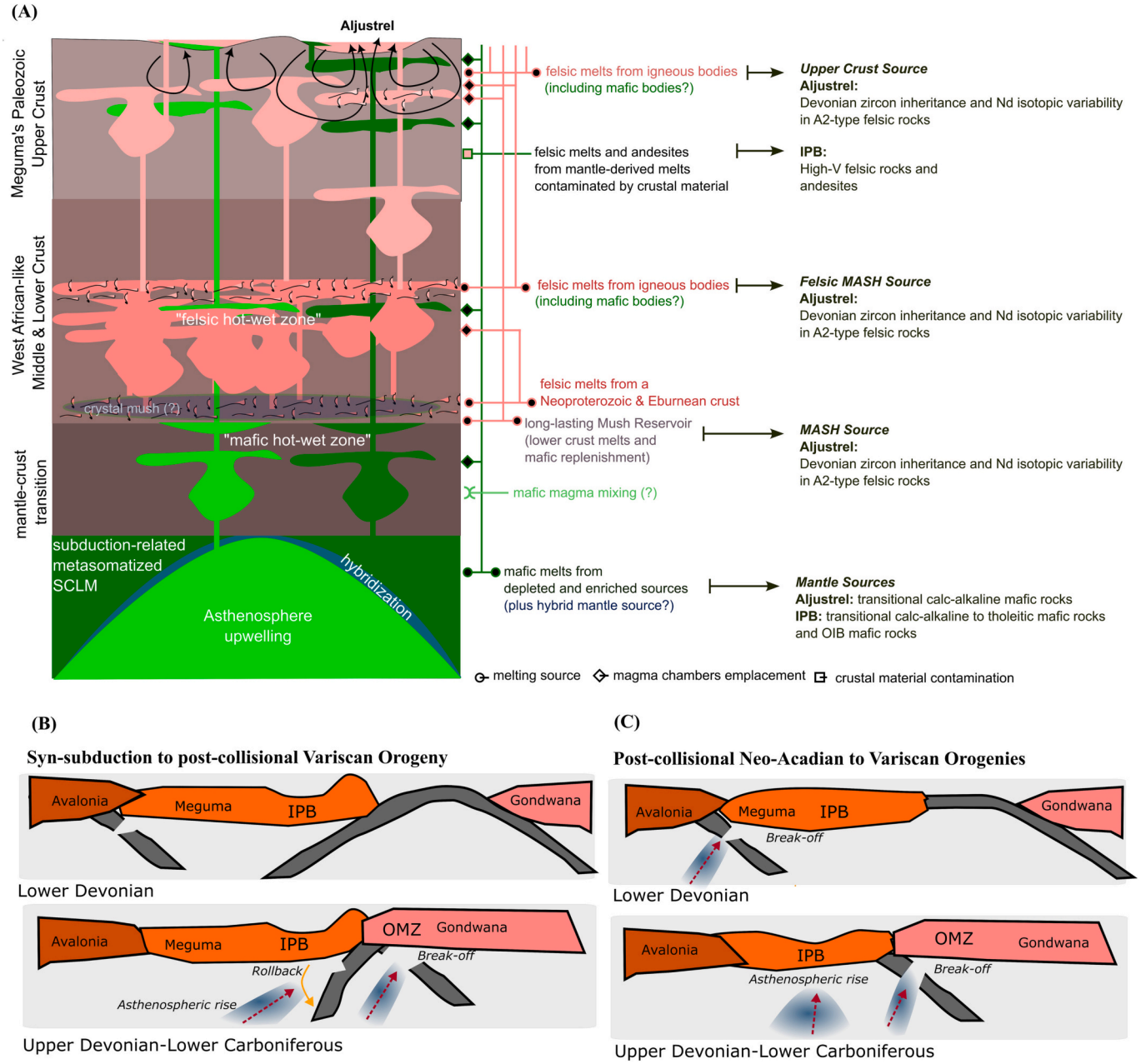

Fig. 13. a) Multi-petrogenetic model for the Iberian Pyrite Belt (see text). b) Post-collisional and c) back-arc geodynamic model for the Iberian Pyrite Belt (see text).

homogenization of the melts extracted from heterogeneous crustal sources, and, thus, in this scenario, the isotopic Nd variability register in the volcanic rock of Aljustrel can be related to a diversely isotopic source.

Alternatively to middle-lower crustal melting, the incorporation of antecrysts into the felsic melt at shallower levels (i.e., upper crust) has also been shown to occur (Bindeman and Simakin, 2014). These authors noticed that in some recent volcanic centers the $\delta^{18}O$ in zircon and whole-rock have relatively low values, suggesting that the low, but diverse, $\delta^{18}O$ in zircon was inherited from the remelting of igneous rocks (plutons or feeding channels) that acquired lower $\delta^{18}O$ bulk chemistry due to meteoric circulation. According to the same authors, remelting of pre-existing Si-rich igneous rocks is an easier and faster process than crustal melting at the lower crust by underplating mafic magmas. In addition, partial melting of the upper crust has been suggested by several authors for the origin of Si-rich IPB magmatism (Codeço et al., 2018; Mitjavila et al., 1997; Rosa et al., 2004; Valenzuela et al., 2011b). Taken together, remelting of previous igneous bodies is also a valid mechanism to explain the zircon antecrysts of the volcanic rocks instead of protracted periods of melt incubation in the lower crust.

5.2.5. *Petrogenetic and geodynamic inferences*

The protracted magmatic history of the IPB, from ~390 Ma, or even as early as ~415 Ma (Feitoza et al., 2023; Lains Amaral et al., 2021a; Pereira et al., 2021; Solá et al., 2015), to 340 Ma (Barrie et al., 2002; Paslawski et al., 2020), was most likely very complex with generation of melts at several levels of the crust, concomitant with the ascent of mantle-derived magmas that might not have interacted with felsic melts during this protracted period, but were considerably important in providing heat at different crustal levels (Fig. 13a) and, ultimately, related to the heat of the hydrothermal system (Yesares et al., 2023). In Fig. 13a, an attempt was made to summarize the multiple possible processes that could explain the isotopic variability and geochemical signatures, namely the A2-type, of the felsic volcanic rocks, as well as the enriched and depleted mantle-derived signatures.

Considering that the petrogenetic models addressed in the previous section are, indeed, plausible for the genesis of the felsic volcanism in the IPB (see also Fig. 13a), in this work, we proposed a hybrid model that accounts isotopic diversity, abundant zircon inheritance and A2-type signature observed in the felsic volcanic rocks of Aljustrel. Firstly, earlier melting was developed in mafic hot-wet zones triggered by the onset of mafic underplating, producing and providing felsic and mafic melts to the middle and lower crust. The felsic melts would carry the isotopic signature of the West-African-like lower crust to the middle crusta. The progressive and long-lived accumulation of granitoids and other melts at the middle crust, forming a felsic MASH zone, would culminate with the necessary heat and water to melt previous hydrous mineral-bearing felsic bodies, promoting the generation of isotopic diverse, antecryst-rich, A2-type melts (although the punctual contribution from Devonian-Carboniferous mafic bodies or sediments to the isotopic variability of the melts cannot be ruled out). These felsic melts would rise as upper crust sub-volcanic rocks, that could be further remelted, or in volcanic extrusions. This sequence of geologic events may have promoted the successive metal remobilization and their anomalous concentration, making the IPB a unique metallogenetic province.

In this petrogenetic context and considering the subduction-related and OIB signatures of the IPB mafic rocks, a geodynamic model involving asthenosphere rise related to disturbances of the subduction system (e.g., break-off, tearing, roll-back, ridge-subduction) must be considered. Recently, an extensive review of IPB volcanic ages suggested that volcanism defined subparallel axes that become younger to the NE, and along each axis, younger to SE-E (Albardeiro et al., 2023). In one of their models, these authors suggested that migration of volcanic activity to the NE in the IPB was related to a hot spot. However, asthenosphere upwelling as a result of slab break-off could also provide the "deep-seated heat source" as stated by the authors. In this regard, a geodynamic model involving asthenosphere rise in response to subduction cessation under Meguma related to the Neo-Acadian Orogeny (Bickerton et al., 2022; Van Staal et al., 2009), followed by an intracontinental extensional setting as the result of the Variscan collision of Gondwana with Meguma can be also envisaged (Fig. 12c). However, the decrease in age of the volcanic activity from SW to NE (closer to the SW Iberian suture) is more likely related to variations of slab dip in a back-arc setting (see e.g., Caratori Tontini et al., 2019; Gallhofer et al., 2015; Nicholson et al., 2004). In this regard, the IPB is envisaged as being formed in a marginal basin (Munhá, 1983; Rubio Pascual et al., 2013; Tornos et al., 2015), in which steepening of the slab (e.g.: roll-back), coupled with slab tearing, promoted migration of the volcanic centers to the trench and to the side (Fig. 12b). This implies a long-lasting subduction setting, since the Lower Devonian, dipping southwards (present coordinates), and that complete closure of the ocean between Ossa-Morena Zone and South Portuguese Zone (Meguma) is likely not prior to the Carboniferous, favoring complex geodynamic models for the latest stages of oceanic closure in southern Iberia (Lains Amaral et al., 2022a; Murphy et al., 2016) (Fig. 12b).

6. Conclusions

The main conclusions of this work regarding the Aljustrel district of the IPB, based on whole-rock immobile trace elements and isotopic study, supported by geochronology, are:

1) Immobility/mobility of certain ratios or elements under hydrothermal alteration should be carried out in well-established chemotypes. HREE may have been partly mobile, and Ga was shown to behave mostly as immobile.
2) The felsic rocks of Aljustrel have Ga/Al and Y/Nb ratios of A2-melts and $(La/Yb)_N^C$ ratios of FII melts.
3) Slight radiogenic initial isotopic values points that most mafic Aljustrel rocks might have had some degree of contamination by crustal material, but one high radiogenic sample argues against a significant role of crustal contamination, suggesting that the geochemical signatures of these rocks were derived from the mantle.
4) The Aljustrel mafic rocks show a calc-alkaline affinity and their orogenic signatures, namely Nb-Ta-Ti negative anomalies, are attributed to an enriched mantle source.
5) Felsic rocks have moderate unradiogenic to slightly radiogenic Sm—Nd isotopic signatures, yielding two-stage model ages that are in accordance with previously obtained two-stage model ages of Lu—Hf in zircon.
6) Previous studies show that the slight to moderate unradiogenic chemotype contains a significant antecrysts population. In this work, abundant antecryts were also detected in the more juvenile felsic rocks, suggesting that remelting of previous igneous rocks was a significant petrogenetic process in all felsic volcanism in Aljustrel. Notwithstanding, few xenocrysts identified in previous studies suggest minor contribution of metasedimentary rocks.
7) The isotopic variability and the A2-type signature could have resulted from melting of isotopically variable igneous felsic rocks with or without the involvement of mafic igneous intrusions. In turn, the isotopic variability of the source might have resulted from melting of an isotopically diverse meta-igneous and meta-sedimentary lower crust.
8) The combined mafic and felsic geochemical signatures of the IPB volcanic rocks point to a geodynamic setting associated to asthenospheric rise that can be either related to i) slab break-off in response to the Neo-Acadian collision between Meguma and Avalonia (Laurussia), soon followed by the Variscan collision between Gondwana and Meguma (Laurussia) or ii) roll-back and tearing of the subducted oceanic crust formed between Gondwana and Meguma.

CRediT authorship contribution statement

João Lains Amaral: Conceptualization, Methodology, Investigation, Writing – original draft, Writing – review & editing, Visualization. **Ana Rita Solá:** Supervision, Writing – review & editing. **Telmo M. Bento dos Santos:** Supervision, Writing – review & editing. **Lorena Feitoza:** Investigation. **Colombo Tassinari:** Resources, Funding acquisition. **Lourenço Crispim:** Investigation. **Martim Chichorro:** Investigation, Writing – review & editing. **Mandy Zieger-Hofmann:** Investigation. **Jessica Gärtner:** Investigation. **Ulf Linnemann:** Resources, Funding acquisition. **João Gonçalves:** Resources, Funding acquisition.

Declaration of competing interest

The authors declare that they have no known competing financial interests or personal relationships that could have appeared to influence the work reported in this paper.

Acknowledgements

We are sincerely grateful the two anonymous reviewers for their substantial and insightful reviews that improved the manuscript and Astrid Holzheid for editorial handling. João Lains Amaral is thankful for all the support from Cristina Pereira at the Alminas's core shed, as well as mine geologists and helpers. In addition, he thanks Filipe Nobre for the discussion and identification of some lithotypes in Aljustrel and Carlos Rosa for discussion on some volcanic textures. We thank Orica for the access to their installations and the availability of Nuno Teixeira. This work acknowledges the support of FCT through PhD grant SFRH/BD/138791/2018 to João Lains Amaral and funding by the Portuguese Fundação para a Ciência e a Tecnologia (FCT) I.P./MCTES through national funds (PIDDAC) – UIDB/50019/2020.

Appendix A. Supplementary data

Supplementary data to this article can be found online at https://doi.org/10.1016/j.chemer.2023.126049.

References

Albardeiro, L., Morais, I., Matos, J.X., Solá, R., Salgueiro, R., Pereira, Z., Mendes, M., Batista, M.J., de Oliveira, D., Díez-Montes, A., Inverno, C., Pacheco, N., Araújo, V., 2023. Time-space evolution of Iberian Pyrite Belt igneous activity: volcanic and plutonic lineaments, geochronology, ore horizons and stratigraphic constraints. Gondwana Res. 121, 235–258. https://doi.org/10.1016/j.gr.2023.05.004.

Andrade, R.F., Schermerhorn, L.J.G., 1971. Aljustrel e Gavião. In: Carvalho, D., Goinhas, J.A.C., Schermerhorn, L.J.G. (Eds.), Principais Jazigos Minerais Do Sul de Portugal. Direcção-Geral de Minas e Serviços Geológicos, Lisboa, pp. 32–59.

Annen, C., Blundy, J.D., Sparks, R.S.J., 2006. The genesis of intermediate and silicic magmas in deep crustal hot zones. J. Petrol. 47, 505–539. https://doi.org/10.1093/petrology/egi084.

Archibald, D.B., Macquarrie, L.M.G., Murphy, J.B., Strachan, R.A., McFarlane, C.R.M., Button, M., Larson, K.P., Dunlop, J., 2021. The construction of the Donegal composite batholith. Temporal constraints from U-Pb dating of zircon and titanite. GSA Bulletin, Irish Caledonides. https://doi.org/10.1130/b35856.1.

Azor, A., Rubatto, D., Simancas, J.F., González Lodeiro, F., Martínez Poyatos, D., Martín Parra, L.M., Matas, J., 2008. Rheic Ocean ophiolitic remnants in southern Iberia questioned by SHRIMP U-Pb zircon ages on the Beja-Acebuches amphibolites. Tectonics 27, TC5006. https://doi.org/10.1029/2008TC002306.

Ballouard, C., Massuyeau, M., Elburg, M.A., Tappe, S., Viljoen, F., Brandenburg, J.-T., 2020. The magmatic and magmatic-hydrothermal evolution of felsic igneous rocks as seen through Nb-Ta geochemical fractionation, with implications for the origins of rare-metal mineralizations. Earth Sci. Rev. 203, 103115 https://doi.org/10.1016/j.earscirev.2020.103115.

Barbarin, B., 1990. Granitoids: Main petrogenetic classifications in relation to origin and tectonic setting. Geol. J. 25, 227–238. https://doi.org/10.1002/gj.3350250306.

Barr, S.M., White, C.E., Pin, C., 2022. Revised stratigraphy in the eastern Meguma terrane, Nova Scotia, Canada, and variations in whole-rock chemical and Sm–Nd isotopic compositions of the Goldenville and Halifax groups. Atlantic Geosci. 58, 193–213. https://doi.org/10.4138/atlgeo.2022.008.

Barrett, T., 2008. Chemostratigraphy, Petrography and Alteration of Volcanic Rocks at the Feitais Deposit and in Two Regional Holes, Aljustrel Area, Portugal. Unpublished report for AGC Minas de Portugal Unipessoal Lda, p. 33.

Barrett, T., 2010. Chemostratigraphy and Alteration at the Lombador Deposit. Unpublished report for AGC Minas de Portugal, Neves Corvo, Portugal, p. 24.

Barrett, T.J., 2009. Geology and Chemostratigraphy of Selected 2008 Drillholes at the Gavião. Unpublished report for AGC Minas de Portugal, Feitais and Lousal Deposits, Portugal, p. 33.

Barrett, T.J., Dawson, G.L., MacLean, W.H., 2008. Volcanic stratigraphy, alteration, and sea-floor setting of the Paleozoic Feitais massive sulfide deposit, Aljustrel, Portugal. Econ. Geol. 103, 215–239. https://doi.org/10.2113/gsecongeo.103.1.215.

Barrie, T.C., Amelin, Y., Pascual, E., 2002. U–Pb Geochronology of VMS mineralization in the Iberian Pyrite Belt. Mineral. Deposita 37, 684–703. https://doi.org/10.1007/s00126-002-0302-7.

Barriga, F., 1983. Hydrothermal Metamorphism and Ore Genesis at Aljustrel. Unpublished PhD, University Ontario, Canada, Portugal, p. 368.

Barriga, F., Kerrich, R., 1984. Extreme 18O-enriched volcanics and 18O-evolved marine water, Aljustrel, Iberian Pyrite Belt: transition from high to low Rayleigh number convective regimes. Geochim. Cosmochim. Acta 48, 1021–1031.

Barriga, F.J.A.S., Fyfe, W.S., 1997. Multi-phase water-rhyolite interaction and ore fluid generation at Aljustrel, Portugal. Mineral. Deposita 33, 188–207. https://doi.org/10.1007/s001260050140.

Bea, F., Morales, I., Molina, J.F., Montero, P., Cambeses, A., 2021. Zircon stability grids in crustal partial melts: implications for zircon inheritance. Contrib. Mineral. Petrol. 176, 18. https://doi.org/10.1007/s00410-021-01772-x.

Bea, F., Montero, P., Barcos, L., Cambeses, A., Molina, J.F., Morales, I., 2023. Understanding Nd model ages of granite rocks: the effects of the 147Sm/144Nd variability during partial melting and crystallization. Lithos 436–437, 106940. https://doi.org/10.1016/j.lithos.2022.106940.

Bento dos Santos, T.M., Munhá, J.M., Tassinari, C.C.G., Fonseca, P.E., 2011. The link between partial melting, granitization and granulite development in central Ribeira Fold Belt, SE Brazil: new evidence from elemental and Sr–Nd isotopic geochemistry. J. S. Am. Earth Sci. 31, 262–278. https://doi.org/10.1016/j.jsames.2011.01.004.

Bickerton, L., Kontak, D.J., Murphy, J.B., Kellett, D.A., Samson, I.M., Marsh, J.H., Dunning, G., Stern, R., 2022. The age and origin of the South Mountain Batholith (Nova Scotia, Canada) as constrained by zircon U–Pb geochronology, geochemistry, and O–Hf isotopes. Can. J. Earth Sci. 59, 418–454. https://doi.org/10.1139/cjes-2021-0097.

Bindeman, I.N., Simakin, A.G., 2014. Rhyolites—hard to produce, but easy to recycle and sequester: integrating microgeochemical observations and numerical models. Geosphere 10, 930–957. https://doi.org/10.1130/GES00969.1.

Bonin, B., 2007. A-type granites and related rocks: evolution of a concept, problems and prospects. Lithos 97, 1–29. https://doi.org/10.1016/j.lithos.2006.12.007.

Bonin, B., Janoušek, V., Moyen, J.-F., 2020. Chemical variation, modal composition and classification of granitoids. In: Geological Society, London, Special Publications 491, 9 LP – 51. https://doi.org/10.1144/SP491-2019-138.

Bouvier, A., Vervoort, J.D., Patchett, P.J., 2008. The Lu–Hf and Sm–Nd isotopic composition of CHUR: constraints from unequilibrated chondrites and implications for the bulk composition of terrestrial planets. Earth Planet. Sci. Lett. 273, 48–57. https://doi.org/10.1016/j.epsl.2008.06.010.

Braid, J.A., Murphy, J.B., Quesada, C., Mortensen, J., 2011. Tectonic escape of a crustal fragment during the closure of the Rheic Ocean: U–Pb detrital zircon data from the Late Palaeozoic Pulo do Lobo and South Portuguese zones, southern Iberia. J. Geol. Soc. Lond. 168, 383–392. https://doi.org/10.1144/0016-76492010-104.

Braid, J.A., Murphy, J.B., Quesada, C., Bickerton, L., Mortensen, J.K., 2012. Probing the composition of unexposed basement, South Portuguese Zone, southern Iberia: implications for the connections between the Appalachian and Variscan orogens. Can. J. Earth Sci. 49, 591–613. https://doi.org/10.1139/E11-071.

Cabanis, B., Lecolle, M., 1989. Le diagramme La/10-Y/15-Nb/8: Un outil pour la discrimination des series volcaniques et lamise en evidence des processus demelange et/ou de contamination crustale. C. R. Acad. Sci. Ser. II, 2023–2029.

Cann, J.R., 1970. Rb, Sr, Y, Zr and Nb in some ocean floor basaltic rocks. Earth Planet. Sci. Lett. 10, 7–11. https://doi.org/10.1016/0012-821X(70)90058-0.

Caratori Tontini, F., Bassett, D., de Ronde, C.E.J., Timm, C., Wysoczanski, R., 2019. Early evolution of a young back-arc basin in the Havre Trough. Nat. Geosci. 12, 856–862. https://doi.org/10.1038/s41561-019-0439-y.

Chappell, B.W., White, A.J.R., 1992. I- and S-type granites in the Lachlan Fold Belt. Earth Environ. Sci. Trans. R. Soc. Edinb. 83, 1–26. https://doi.org/10.1017/S0263593300007720.

Chopin, F., Leprêtre, R., El Houicha, M., Tabaud, A.-S., Schulmann, K., Míková, J., Barbarand, J., Chebli, R., 2023. U–Pb geochronology of Variscan granitoids from the Moroccan Meseta (Northwest Africa): tectonic implications. Gondwana Res. 117, 274–294. https://doi.org/10.1016/j.gr.2023.02.004.

Clarke, D.B., Chatterjee, A.K., Giles, P.S., 1993. Petrochemistry, tectonic history, and Sr–Nd systematics of the Liscomb Complex, Meguma Lithotectonic Zone, Nova Scotia. Can. J. Earth Sci. 30, 449–464. https://doi.org/10.1139/e93-033.

Clemens, J.D., Bryan, S.E., Mayne, M.J., Stevens, G., Petford, N., 2022. How are silicic volcanic and plutonic systems related? Part 1: a review of geological and geophysical observations, and insights from igneous rock chemistry. Earth Sci. Rev. 235, 104249 https://doi.org/10.1016/j.earscirev.2022.104249.

Codeço, M.S., Mateus, A., Figueiras, J., Rodrigues, P., Gonçalves, L., 2018. Development of the Ervidel-Roxo and Figueirinha-Albernoa volcanic sequences in the Iberian pyrite Belt, Portugal: Metallogenic and geodynamic implications. Ore Geol. Rev. 98, 80–108. https://doi.org/10.1016/J.OREGEOREV.2018.05.009.

Collins, W.J., Beams, S.D., White, A.J.R., Chappell, B.W., 1982. Nature and origin of A-type granites with particular reference to southeastern Australia. Contrib. Mineral. Petrol. 80, 189–200. https://doi.org/10.1007/BF00374895.

Conde, C., Tornos, F., 2020. Geochemistry and architecture of the host sequence of the massive sulfides in the northern Iberian Pyrite Belt. Ore Geol. Rev. 127, 103042 https://doi.org/10.1016/j.oregeorev.2019.103042.
Condie, K.C., Pisarevsky, S.A., Puetz, S.J., Roberts, N.M.W., Spencer, C.J., 2023. A-type granites in space and time: relationship to the supercontinent cycle and mantle events. Earth Planet. Sci. Lett. 610, 118125 https://doi.org/10.1016/j.epsl.2023.118125.
De Campos, C.P., Perugini, D., Ertel-Ingrisch, W., Dingwell, D.B., Poli, G., 2011. Enhancement of magma mixing efficiency by chaotic dynamics: an experimental study. Contrib. Mineral. Petrol. 161, 863–881. https://doi.org/10.1007/s00410-010-0569-0.
de la Rosa, J.D., Jenner, G.A., Castro, A., 2002. A study of inherited zircons in granitoid rocks from the South Portuguese and Ossa-Morena Zones, Iberian Massif: support for the exotic origin of the South Portuguese Zone. Tectonophysics 352, 245–256. https://doi.org/10.1016/S0040-1951(02)00199-3.
de Mello, C.R., Tornos, F., Conde, C., Tassinari, C.C.G., Farci, A., Vega, R., 2022. Geology, Geochemistry, and Geochronology of the Giant Rio Tinto VMS Deposit, Iberian Pyrite Belt, Spain. Econ. Geol. 117, 1149–1177. https://doi.org/10.5382/econgeo.4907.
DePaolo, D.J., Wasserburg, G.J., 1979. Petrogenetic mixing models and Nd-Sr isotopic patterns. Geochim. Cosmochim. Acta 43, 615–627. https://doi.org/10.1016/0016-7037(79)90169-8.
Dias da Silva, Í., Pereira, M.F., Silva, J.B., Gama, C., 2018. Time-space distribution of silicic plutonism in a gneiss dome of the Iberian Variscan Belt: the Évora Massif (Ossa-Morena Zone, Portugal). Tectonophysics 747–748, 298–317. https://doi.org/10.1016/J.TECTO.2018.10.015.
Donaire, T., Pascual, E., Sáez, R., Pin, C., Hamilton, M.A., Toscano, M., 2020a. Geochemical and Nd isotopic signature of felsic volcanic rocks as a proxy of volcanic-hosted massive sulphide deposits in the Iberian Pyrite Belt (SW, Spain): the Paymogo Volcano-Sedimentary Alignment. Ore Geol. Rev. 120, 103408 https://doi.org/10.1016/j.oregeorev.2020.103408.
Donaire, T., Pascual, E., Sáez, R., Toscano, M., 2020b. Facies architecture and palaeoenvironmental constraints of subaqueous felsic volcanism in the Iberian Pyrite Belt: the Paymogo Volcano-Sedimentary Alignment. J. Volcanol. Geotherm. Res. 405, 107045 https://doi.org/10.1016/j.jvolgeores.2020.107045.
dos Santos, R.S.R., 2021. Padrões de Alteração Hidrotermal/Mineralização no Sector W do Jazigo de Sulfuretos Maciços Polimetálicos do Gavião – Aljustrel. Unpublished Msc, Universidade de Lisboa, Portugal, p. 167.
Dostal, J., Keppie, D.J., Jutras, P., Miller, B.V., Murphy, B.J., 2006. Evidence for the granulite–granite connection: penecontemporaneous high-grade metamorphism, granitic magmatism and core complex development in the Liscomb Complex, Nova Scotia, Canada. Lithos 86, 77–90. https://doi.org/10.1016/j.lithos.2005.04.002.
Eberz, G.W., Clarke, D.B., Chatterjee, A.K., Giles, P.S., 1991. Chemical and isotopic composition of the lower crust beneath the Meguma Lithotectonic Zone, Nova Scotia: evidence from granulite facies xenoliths. Contrib. Mineral. Petrol. 109, 69–88. https://doi.org/10.1007/BF00687201.
Eby, G.N., 1992. Chemical subdivision of the A-type granitoids: petrogenetic and tectonic implications. Geology 20, 641–644. https://doi.org/10.1130/0091-7613(1992)020<0641:CSOTAT>2.3.CO;2.
Farina, F., Stevens, G., Gerdes, A., Frei, D., 2014. Small-scale Hf isotopic variability in the Peninsula pluton (South Africa): the processes that control inheritance of source 176Hf/177Hf diversity in S-type granites. Contrib. Mineral. Petrol. 168, 1065. https://doi.org/10.1007/s00410-014-1065-8.
Fassbender, M.L., Hannington, M., Stewart, M., Brandl, P.A., Baxter, A.T., Diekrup, D., 2022. Geochemical signatures of felsic volcanic rocks in modern oceanic settings and implications for Archean greenstone belts. Econ. Geol. https://doi.org/10.5382/econgeo.4967.
Feitoza, L.M., Bento dos Santos, T., Lains Amaral, J., Solá, A.R., Tassinari, C.C.G., Basei, M.A.S., Matos, J.X., Albardeiro, L., Morais, I., 2023. The oldest magmatism of the Iberian Pyrite Belt: U-Pb geochronological data from the Salgadinho deposit, Cercal. In: Resumos Do XI CNG 2023, Coimbra, 17–19 de Julho de 2023.
Frost, B.R., Frost, C.D., 2008. A geochemical classification for feldspathic igneous rocks. J. Petrol. 49, 1955–1969. https://doi.org/10.1093/petrology/egn054.
Frost, B.R., Barnes, C.G., Collins, W.J., Arculus, R.J., Ellis, D.J., Frost, C.D., 2001. A geochemical classification for granitic rocks. J. Petrol. 42, 2033–2048. https://doi.org/10.1093/petrology/42.11.2033.
Frost, C., Frost, B., Beard, J., 2016. On silica-rich granitoids and their eruptive equivalents. Am. Mineral. 101 (6), 1268–1284. https://doi.org/10.2138/am-2016-5307.
Gallhofer, D., Quadt, A. von, Peytcheva, I., Schmid, S.M., Heinrich, C.A., 2015. Tectonic, magmatic, and metallogenic evolution of the Late Cretaceous arc in the Carpathian-Balkan orogen. Tectonics 34, 1813–1836. https://doi.org/10.1002/2015TC003834.
Gao, P., Zheng, Y., Zhao, Z., 2016. Experimental melts from crustal rocks: a lithochemical constraint on granite petrogenesis. Lithos 266–267, 133–157. https://doi.org/10.1016/j.lithos.2016.10.005.
Gerdes, A., Zeh, A., 2006. Combined U–Pb and Hf isotope LA-(MC-)ICP-MS analyses of detrital zircons: comparison with SHRIMP and new constraints for the provenance and age of an Armorican metasediment in Central Germany. Earth Planet. Sci. Lett. 249, 47–61. https://doi.org/10.1016/j.epsl.2006.06.039.
Gifkins, C., Herrmann, W., Large, R., 2006. Altered Volcanic Rocks; a Guide to Description and Interpretation., Economic Geology. CODES-Centre for Ore Deposit Research, University of Tasmania.
Gisbert, G., Tornos, F., Losantos, E., Pons, J.M., Videira, J.C., 2021. Vectors to ore in replacive volcanogenic massive sulfide (VMS) deposits of the northern Iberian Pyrite Belt: mineral zoning, whole rock geochemistry, and application of portable X-ray fluorescence. Solid Earth 12, 1931–1966. https://doi.org/10.5194/se-12-1931-2021.
Griffin, W.L., Wang, X., Jackson, S.E., Pearson, N.J., O'Reilly, S.Y., Xu, X., Zhou, X., 2002. Zircon chemistry and magma mixing, SE China: in-situ analysis of Hf isotopes, Tonglu and Pingtan igneous complexes. Lithos 61, 237–269. https://doi.org/10.1016/S0024-4937(02)00082-8.
Hannington, M.D., De Ronde, C.E.J., Petersen, S., 2005. Sea-floor Tectonics and Submarine Hydrothermal Systems.
Hart, T.R., Gibson, H.L., Lesher, C.M., 2004. Trace element geochemistry and petrogenesis of felsic volcanic rocks associated with volcanogenic massive Cu-Zn-Pb sulfide deposits. Econ. Geol. 99, 1003–1013. https://doi.org/10.2113/gsecongeo.99.5.1003.
Hiess, J., Condon, D.J., McLean, N., Noble, S.R., 2012. 238U/235U systematics in terrestrial uranium-bearing minerals. Science 1979 (335), 1610–1614. https://doi.org/10.1126/science.1215507.
Hildreth, W., Moorbath, S., 1988. Crustal contributions to arc magmatism in the Andes of Central Chile. Contrib. Mineral. Petrol. 98, 455–489. https://doi.org/10.1007/BF00372365.
Hoseong, L., Oliver, N., F, W.R., Yona, N.-J., R, B.V., Jongkyu, P., Bora, M., A, C.P., 2024. Lower crustal hot zones as zircon incubators: inherited zircon antecryts in diorites from a mafic mush reservoir. Geol. Soc. Lond. Spec. Publ. 537, SP537-2021–195 https://doi.org/10.1144/SP537-2021-195.
Huston, D.L., Relvas, J.M.R.S., Gemmell, J.B., Drieberg, S., 2011. The role of granites in volcanic-hosted massive sulphide ore-forming systems: an assessment of magmatic–hydrothermal contributions. Mineral. Deposita 46, 473–507. https://doi.org/10.1007/s00126-010-0322-7.
Inverno, C.M.C., Solomon, M., Barton, M.D., Foden, J., 2008. The Cu stockwork and massive sulfide ore of the Feitais volcanic-hosted massive sulfide deposit, Aljustrel, Iberian Pyrite Belt, Portugal: a mineralogical, fluid inclusion, and isotopic investigation. Econ. Geol. 103, 241–267. https://doi.org/10.2113/gsecongeo.103.1.241.
Irvine, T.N., Baragar, W.R.A., 1971. A guide to the chemical classification of the common volcanic rocks. Can. J. Earth Sci. 8, 523–548. https://doi.org/10.1139/e71-055.
Ishibashi, J., Ikegami, F., Tsuji, T., Urabe, T., 2015. Hydrothermal activity in the Okinawa Trough back-arc basin: geological background and hydrothermal mineralization. In: Ishibashi, J., Okino, K., Sunamura, M. (Eds.), Subseafloor Biosphere Linked to Hydrothermal Systems: TAIGA Concept. Springer Japan, Tokyo, pp. 337–359. https://doi.org/10.1007/978-4-431-54865-2_27.
Jackson, M.D., Blundy, J., Sparks, R.S.J., 2018. Chemical differentiation, cold storage and remobilization of magma in the Earth's crust. Nature 564, 405–409. https://doi.org/10.1038/s41586-018-0746-2.
Jaffey, A.H., Flynn, K.F., Glendenin, L.E., Bentley, W.C., Essling, A.M., 1971. Precision measurement of half-lives and specific activities of $^{235}\mathrm{U}$ and $^{238}\mathrm{U}$. Phys. Rev. C 4, 1889–1906. https://doi.org/10.1103/PhysRevC.4.1889.
Janoušek, V., Farrow, C.M., Erban, V., 2006. Interpretation of whole-rock geochemical data in igneous geochemistry: introducing Geochemical Data Toolkit (GCDkit). J. Petrol. 47, 1255–1259.
Jorge, R., Relvas, J., Matos, J., 2006. Geochemistry of metasediments from the phyllite–quartzite group, Iberian Pyrite Belt: provenance, source-area weathering and geotectonic implications. Geochim. Cosmochim. Acta 70, A298.
Kerr, A., Fryer, B.J., 1993. Nd isotope evidence for crust-mantle interaction in the generation of A-type granitoid suites in Labrador, Canada. Chem. Geol. 104, 39–60. https://doi.org/10.1016/0009-2541(93)90141-5.
Lains Amaral, J., Solá, A., Bento dos Santos, T., 2021a. Inspecting zircon populations of the Iberian Pyrite Belt: tracking the Cadomian record of the South Portuguese Zone. In: Álvaro, J.J., Chichorro, M., Gutiérrez-Alonso, G. (Eds.), The Panafrican and Cadomian Orogenies in North Africa and Western Europe, p. 8. https://doi.org/10.5281/ZENODO.5084628.
Lains Amaral, J., Solá, A.R., Bento dos Santos, T.M., Tassinari, C.C.G., Gonçalves, J., 2021b. U-Pb zircon SHRIMP dating of a protracted magmatic setting and its volcanic emplacement: insights from the felsic volcanic rocks hosting the sulphide ore of the giant Aljustrel Deposit, Iberian Pyrite Belt. Ore Geol. Rev. 134, 104147 https://doi.org/10.1016/j.oregeorev.2021.104147.
Lains Amaral, J., Ferreira, E., Solá, A.R., Bento dos Santos, T.M., Albardeiro, L., Gonçalves, J., 2024. Zircon separation workflow: methods, techniques and bias - lessons from drill core samples of the volcanic rocks of the Iberian Pyrite Belt. Geonovas (in press).
Lains Amaral, J., Mata, J., Santos, J.F., 2022a. The Carboniferous shoshonitic (s.l.) gabbro–monzonitic stocks of Veiros and Vale de Maceira, Ossa-Morena Zone (SW Iberian Massif): evidence for diverse subduction-related lithospheric metasomatism. Geochemistry 82, 125917. https://doi.org/10.1016/j.chemer.2022.125917.
Lains Amaral, J., Solá, A.R., Bento dos Santos, T.M., Chichorro, M., 2022b. Detrital zircon similarities and dissimilarities between the Iberian Pyrite Belt, Ossa-Morena Zone and Meguma. Geol. Acta 20, 1–10. https://doi.org/10.1344/GeologicaActa2022.20.16.
Lang, M., Zhang, Z., Chen, Z., Cheng, Z., Santosh, M., Kusky, T.M., 2023. Classification and nomenclature of volcanic rocks using immobile elements: a novel approach based on big data analysis. Lithos 454–455, 107274. https://doi.org/10.1016/j.lithos.2023.107274.
Large, R.R., Gemmell, J.B., Paulick, H., Huston, D.L., 2001. The alteration box plot: a simple approach to understanding the relationship between alteration mineralogy and lithogeochemistry associated with volcanic-hosted massive sulfide deposits. Econ. Geol. 96, 957–971. https://doi.org/10.2113/gsecongeo.96.5.957.

Le Bas, M.J., Le Maitre, R.W., Streckeisen, A., Zanettin, B., 1986. A chemical classification of volcanic rocks based on the total alkali-silica diagram. J. Petrol. 27, 745–750. https://doi.org/10.1093/petrology/27.3.745.

Leat, P.T., Jackson, S.E., Thorpe, R.S., Stillman, C.J., 1986. Geochemistry of bimodal basalt-subalkaline/peralkaline rhyolite provinces within the Southern British Caledonides. J. Geol. Soc. Lond. 143, 259–273. https://doi.org/10.1144/gsjgs.143.2.0259.

Leistel, J.M., Marcoux, E., Thiéblemont, D., Quesada, C., Sánchez, A., Almodóvar, G.R., Pascual, E., 1997. The volcanic-hosted massive sulphide deposits of the Iberian Pyrite Belt Review and preface to the Thematic Issue. Mineral. Deposita 33, 2–30. https://doi.org/10.1007/s001260050130.

Leitão, J.C., 2009. Geodinâmica varisca, vulcano-sedimentar e tectónica, na área de Aljustrel. Unpublished PhD.Universidade de Trás-os-Montes e Alto Douro, Portugal, p. 448.

Liew, T.C., Hofmann, A.W., 1988. Precambrian crustal components, plutonic associations, plate environment of the Hercynian Fold Belt of central Europe: indications from a Nd and Sr isotopic study. Contrib. Mineral. Petrol. 98, 129–138. https://doi.org/10.1007/BF00402106.

Lugmair, G.W., Marti, K., 1978. Lunar initial 143Nd/144Nd: differential evolution of the lunar crust and mantle. Earth Planet. Sci. Lett. 39, 349–357. https://doi.org/10.1016/0012-821X(78)90021-3.

Luz, F., Mateus, A., Ferreira, E., Tassinari, C.G., Figueiras, J., 2022. Pb-Nd-Sr isotope geochemistry of metapelites from the Iberian Pyrite Belt and its relevance to provenance analysis and mineral exploration surveys. Econ. Geol. 117, 423–454. https://doi.org/10.5382/econgeo.4869.

MacLean, W.H., Barrett, T.J., 1993. Lithogeochemical techniques using immobile elements. J. Geochem. Explor. 48, 109–133. https://doi.org/10.1016/0375-6742(93)90002-4.

Maniar, P.D., Piccoli, P.M., 1989. Tectonic discrimination of granitoids. GSA Bull. 101, 635–643. https://doi.org/10.1130/0016-7606(1989)101<0635:TDOG>2.3.CO;2.

Marques, A.F.A., Relvas, J.M.R.S., Scott, S.D., Rosa, C., Guillong, M., 2020. Melt inclusions in quartz from felsic volcanic rocks of the Iberian Pyrite Belt: clues for magmatic ore metal transfer towards VMS-forming systems. Ore Geol. Rev. 126, 103743 https://doi.org/10.1016/j.oregeorev.2020.103743.

Martin-Izard, A., Arias, D., Arias, M., Gumiel, P., Sanderson, D.J., Castañon, C., Sanchez, J., 2016. Ore deposit types and tectonic evolution of the Iberian Pyrite Belt: from transtensional basins and magmatism to transpression and inversion tectonics. Ore Geol. Rev. 79, 254–267. https://doi.org/10.1016/j.oregeorev.2016.05.011.

Mello, C.R. De, Tassinari, C.C.G., Tornos, F., 2018. U/PB geochronology of the igneous rocks associated to VMS deposits of the Spanish Iberian Pyrite Belt. In: X Congresso Nacional de Geologia;VULCANICA - Revista Portuguesa de Vulcanologia, pp. 259–260.

Mendes, M., Pereira, Z., Matos, J.X., Albardeiro, L., Morais, I., Solá, R., Pacheco, N., Araújo, V., 2018. Middle-Upper Devonian palynostratigraphy of the Phyllite-Quartzite Group in the Neves-Corvo Mine Region, Iberian Pyrite Belt - correlation with the South Portuguese Zone. In: Vaz, N., Sá, A.A. (Eds.), Yacimientos Paleontológicos Excepcionales En La Península Ibérica. Cuadernos del MuseoGeominero, 27. Instituto Geológico y Minero de España, Madrid.

Middlemost, E.A.K., 1994. Naming materials in the magma/igneous rock system. Earth Sci. Rev. https://doi.org/10.1016/0012-8252(94)90029-9.

Miles, A.J., Woodcock, N.H., 2018. A combined geochronological approach to investigating long lived granite magmatism, the Shap granite, UK. Lithos 304–307, 245–257. https://doi.org/10.1016/j.lithos.2018.02.012.

Mitjavila, J., Marti, J., Soriano, C., 1997. Magmatic evolution and tectonic setting of the Iberian Pyrite Belt volcanism. J. Petrol. 38, 727–755. https://doi.org/10.1093/petroj/38.6.727.

Miyashiro, A., 1974. Volcanic rock series in island arcs and active continental margins. Am. J. Sci. 274, 321–355. https://doi.org/10.2475/ajs.274.4.321.

Morais, I., Albardeiro, L., Batista, M.J., Matos, J.X., Solá, R., de Oliveira, D.P.S., Salgueiro, R., Araújo, V., Pacheco, N., 2020. Geochemistry of Iberian Pyrite Belt Portuguese sector massive sulfide deposits-related volcanic rocks. Considerations on hydrothermal alteration, petrology and tectonic evolution.

Moreno, C., Sierra, S., Sáez, R., 1996. Evidence for catastrophism at the Famennian-Dinantian boundary in the Iberian Pyrite Belt. Geol. Soc. Lond. Spec. Publ. 107, 153 LP–162. https://doi.org/10.1144/GSL.SP.1996.107.01.12.

Munhá, J., 1983. Hercynian magmatism in the Iberian pyrite belt. In: Comunicacões dos Servicos Geológicos de Portugal, pp. 39–81.

Munhá, J., Kerrich, R., 1980. Sea water basalt interaction in spilites from the Iberian Pyrite Belt. Contrib. Mineral. Petrol. 73, 191–200. https://doi.org/10.1007/BF00371394.

Murphy, J.B., Nance, R.D., 2002. Sm–Nd isotopic systematics as tectonic tracers: an example from West Avalonia in the Canadian Appalachians. Earth Sci. Rev. 59, 77–100. https://doi.org/10.1016/S0012-8252(02)00070-3.

Murphy, J.B., Braid, J.A., Quesada, C., Dahn, D., Gladney, E., Dupuis, N., 2016. An eastern Mediterranean analogue for the Late Palaeozoic evolution of the Pangaean suture zone in SW Iberia. Geol. Soc. Lond. Spec. Publ. 424, 241–263. https://doi.org/10.1144/SP424.9.

Nakamura, N., 1974. Determination of REE, Ba, Fe, Mg, Na and K in carbonaceous and ordinary chondrites. Geochim. Cosmochim. Acta 38, 757–775. https://doi.org/10.1016/0016-7037(74)90149-5.

Nicholson, K.N., Black, P.M., Hoskin, P.W.O., Smith, I.E.M., 2004. Silicic volcanism and back-arc extension related to migration of the Late Cainozoic Australian–Pacific plate boundary. J. Volcanol. Geotherm. Res. 131, 295–306. https://doi.org/10.1016/S0377-0273(03)00382-2.

Ohta, T., Arai, H., 2007. Statistical empirical index of chemical weathering in igneous rocks: a new tool for evaluating the degree of weathering. Chem. Geol. 240, 280–297. https://doi.org/10.1016/j.chemgeo.2007.02.017.

Oliveira, J.T., Pereira, Z., Carvalho, P., Pacheco, N., Korn, D., 2004. Stratigraphy of the tectonically imbricated lithological succession of the Neves Corvo mine area, Iberian Pyrite Belt, Portugal. Mineral. Deposita 39, 422–436. https://doi.org/10.1007/s00126-004-0415-2.

Oliveira, J.T., Rosa, C.J.P., Pereira, Z., Rosa, D.R.N., Matos, J.X., Inverno, C.M.C., Andersen, T., 2013. Geology of the Rosário–Neves Corvo antiform, Iberian Pyrite Belt, Portugal: new insights from physical volcanology, palynostratigraphy and isotope geochronology studies. Mineral. Deposita 48, 749–766. https://doi.org/10.1007/s00126-012-0453-0.

Oliveira, J.T., Quesada, C., Pereira, Z., Matos, J.X., Solá, A.R., Rosa, D., Albardeiro, L., Díez-Montes, A., Morais, I., Inverno, C., Rosa, C., Relvas, J., 2019. South Portuguese terrane: a continental affinity exotic unit. In: Quesada, Cecilio, Oliveira, José Tomás (Eds.), The Geology of Iberia: A Geodynamic Approach, Vol. 2. The Variscan Cycle. Springer, Cham, pp. 173–206. https://doi.org/10.1007/978-3-030-10519-8_6.

Onézime, J., Charvet, J., Faure, M., Bourdier, J.-L., Chauvet, A., 2003. A new geodynamic interpretation for the South Portuguese Zone (SW Iberia) and the Iberian Pyrite Belt genesis. Tectonics 22, 1027. https://doi.org/10.1029/2002TC001387.

Pascual, E., Donaire, T., Toscano, M., Macías, G., Pin, C., Hamilton, M.A., 2021. Geochemical and Volcanological Criteria in Assessing the Links between Volcanism and VMS Deposits: A Case on the Iberian Pyrite Belt. Minerals, Spain. https://doi.org/10.3390/min11080826.

Paslawski, L.E., Braid, J.A., Quesada, C., McFarlane, C.M., 2020. Geochronology of the Iberian Pyrite Belt and the Sierra Norte Batholith: lower plate magmatism during supercontinent amalgamation? Geol. Soc. Lond. Spec. Publ. 503, SP503-2020–5 https://doi.org/10.1144/SP503-2020-5.

Patiño Douce, A.E., 1997. Generation of metaluminous A-type granites by low-pressure melting of calc-alkaline granitoids. Geology 25, 743–746. https://doi.org/10.1130/0091-7613(1997)025<0743:GOMATG>2.3.CO;2.

Pearce, J.A., 1982. Trace element characteristics of lavas from destructive plate boundaries. In: Thorpe, R.S. (Ed.), Orogenic Andesites and Related Rocks. Wiley Chichester, pp. 525–548.

Pearce, J.A., 2008. Geochemical fingerprinting of oceanic basalts with applications to ophiolite classification and the search for Archean oceanic crust. Lithos 100, 14–48. https://doi.org/10.1016/J.LITHOS.2007.06.016.

Pe-Piper, G., Piper, D.J.W., 1998. Geochemical evolution of Devonian-Carboniferous igneous rocks of the Magdalen basin, Eastern Canada: Pb- and Nd-isotope evidence for mantle and lower crustal sources. Can. J. Earth Sci. 35, 201–221. https://doi.org/10.1139/e97-106.

Pereira, Z., Fernandes, P., Matos, J.X., Jorge, R.C.G.S., Oliveira, J.T., 2018. Stratigraphy of the Northern Pulo do Lobo Domain, SW Iberia Variscides: a palynological contribution. Geobios 51, 491–506. https://doi.org/10.1016/j.geobios.2018.04.001.

Pereira, Z., Matos, J.X., Solá, A.R., Batista, M.J., Salgueiro, R., Rosa, C., Albardeiro, L., Mendes, M., Morais, I., de Oliveira, D., Pacheco, N., Araújo, V., Castelo Branco, J.M., Neto, R., Lains Amaral, J., Inverno, C., Oliveira, J.T., 2021. Geology of the recently discovered massive and stockwork sulphide mineralization at Semblana, Rosa Magra and Monte Branco, Neves–Corvo mine region, Iberian Pyrite Belt, Portugal. Geol. Mag. 1–16 https://doi.org/10.1017/S0016756820001284.

Piercey, S.J., 2010. An overview of petrochemistry in the regional exploration for volcanogenic massive sulphide (VMS) deposits. Geochem. Explor. Environ. Anal. 10, 119–136. https://doi.org/10.1144/1467-7873/09-221.

Piercey, S.J., 2011. The setting, style, and role of magmatism in the formation of volcanogenic massive sulfide deposits. Mineral. Deposita 46, 449–471. https://doi.org/10.1007/s00126-011-0341-z.

Plimer, I.R., de Carvalho, D., 1982. The geochemistry of hydrothermal alteration at the Salgadinho copper deposit, Portugal. Mineral. Deposita 17, 193–211. https://doi.org/10.1007/BF00206470.

Pollock, J.C., Sylvester, P.J., Barr, S.M., 2015. Lu–Hf zircon and Sm–Nd whole-rock isotope constraints on the extent of juvenile arc crust in Avalonia: examples from Newfoundland and Nova Scotia, Canada. Can. J. Earth Sci. 52, 161–181. https://doi.org/10.1139/cjes-2014-0157.

Quesada, C., Braid, J.A., Fernandes, P., Ferreira, P., Jorge, R.S., Matos, J.X., Murphy, J. B., Oliveira, J.T., Pedro, J., Pereira, Z., 2019. SW Iberia Variscan suture zone: oceanic affinity units. In: Quesada, Cecilio, Oliveira, José Tomás (Eds.), The Geology of Iberia: A Geodynamic Approach: Volume 2: The Variscan Cycle. Springer International Publishing, Cham, pp. 131–171. https://doi.org/10.1007/978-3-030-10519-8_5.

Relvas, J.M.R.S., 1991. Estudo Geológico e Metalogenético da Área de Gavião. Unpublished MSc, Universidadde de Lisbo, Baixo Alentejo, p. 208.

Relvas, J.M.R.S., Barriga, F.J.A.S., Ferreira, A., Noiva, P.C., Pacheco, N., Barriga, G., 2006. Hydrothermal alteration and mineralization in the Neves-Corvo volcanic-hosted massive sulfide deposit, Portugal. I. Geology, mineralogy, and geochemistry. Econ. Geol. 101, 753–790. https://doi.org/10.2113/gsecongeo.101.4.753.

Relvas, J.M.R.S., Barriga, F., Carvalho, J.R.S., Pinto, Á.M.M., Matos, J.X., Rosa, C.J.P., Pereira, Z., 2011. Structure, stratigraphy and hydrothermal alteration at the Gavião orebodies, Aljustrel: reconstruction of a dismembered ore-forming system at the Iberian Pyrite Belt and implications for exploration. In: 11th SGA Biennial Meeting: Let's Talk Ore Deposits, pp. 772–774.

Rodrigues, B., Chew, D.M., Jorge, R.C.G.S., Fernandes, P., Veiga-Pires, C., Oliveira, J.T., 2015. Detrital zircon geochronology of the Carboniferous Baixo Alentejo Flysch Group (South Portugal); constraints on the provenance and geodynamic evolution of the South Portuguese Zone. J. Geol. Soc. Lond. 172, 294–308. https://doi.org/10.1144/jgs2013-084.

Rosa, C.J.P., 2007. Facies Architecture of the Volcanic SedimentaryvComplex of the Iberian Pyrite Belt, Portugal and Spain (unpublished PhD thesis).. University of Tasmania, University of Tasmania.
Rosa, C.J.P., McPhie, J., Relvas, J.M.R.S., Pereira, Z., Oliveira, T., Pacheco, N., 2008. Facies analyses and volcanic setting of the giant Neves Corvo massive sulfide deposit, Iberian Pyrite Belt, Portugal. Mineral. Deposita 43, 449–466. https://doi.org/10.1007/s00126-008-0176-4.
Rosa, C.J.P., McPhie, J., Relvas, J.M.R.S., 2010. Type of volcanoes hosting the massive sulfide deposits of the Iberian Pyrite Belt. J. Volcanol. Geotherm. Res. 194, 107–126. https://doi.org/10.1016/J.JVOLGEORES.2010.05.005.
Rosa, D.R.N., Inverno, C.M.C., Oliveira, V.M.J., Rosa, C.J.P., 2004. Geochemistry of volcanic rocks, Albernoa area, Iberian Pyrite Belt, Portugal. Int. Geol. Rev. 46, 366–383. https://doi.org/10.2747/0020-6814.46.4.366.
Rosa, D.R.N., Inverno, C.M.C., Oliveira, V.M.J., Rosa, C.J.P., 2006. Geochemistry and geothermometry of volcanic rocks from Serra Branca, Iberian Pyrite Belt, Portugal. Gondwana Res. 10, 328–339. https://doi.org/10.1016/j.gr.2006.03.008.
Rosa, D.R.N., Finch, A.A., Andersen, T., Inverno, C.M.C., 2009. U–Pb geochronology and Hf isotope ratios of magmatic zircons from the Iberian Pyrite Belt. Mineral. Petrol. 95, 47–69. https://doi.org/10.1007/s00710-008-0022-5.
Ross, P.-S., Bédard, J.H., 2009. Magmatic affinity of modern and ancient subalkaline volcanic rocks determined from trace-element discriminant diagrams. Can. J. Earth Sci. 46, 823–839. https://doi.org/10.1139/E09-054.
Rubio Pascual, F.J., Matas, J., Martín Parra, L.M., 2013. High-pressure metamorphism in the Early Variscan subduction complex of the SW Iberian Massif. Tectonophysics 592, 187–199. https://doi.org/10.1016/J.TECTO.2013.02.022.
Sánchez-España, J., Velasco, F., Yusta, I., 2000. Hydrothermal alteration of felsic volcanic rocks associated with massive sulphide deposition in the northern Iberian Pyrite Belt (SW Spain). Appl. Geochem. 15, 1265–1290. https://doi.org/10.1016/S0883-2927(99)00119-5.
Sato, K., Tassinari, C.C.G., Basei, M.A.S., Júnior, O.S., Onoe, A.T., de Souza, M.D., 2014. Microssonda Iônica de Alta Resolução e de Alta Sensibilidade (SHRIMP IIe/MC) do Instituto de Geociências da Universidade de São Paulo, Brasil: método analítico e primeiros resultados. Geologia USP. Série Científica, 14, pp. 3–18.
Schandl, E.S., Gorton, M.P., 2002. Application of high field strength elements to discriminate tectonic settings in VMS environments. Econ. Geol. 97, 629–642. https://doi.org/10.2113/gsecongeo.97.3.629.
Schermerhorn, L.J.G., 1970. The deposition of volcanics and pyritite in the Iberian Pyrite Belt. Mineral. Deposita 5, 273–279.
Schermerhorn, L.J.G., Zbyszewski, G., Ferreira, O., 1987. Carta Geologica de Portugal 1: 50 000. Noticia Explicativa da Folha 42-D (Aljustrel). Serviços Geológicos de Portugal.
Schwindinger, M., Weinberg, R.F., 2017. A felsic MASH zone of crustal magmas — feedback between granite magma intrusion and in situ crustal anatexis. Lithos 284–285, 109–121. https://doi.org/10.1016/j.lithos.2017.03.030.
Shellnutt, J.G., Dostal, J., 2022. Magmatic and inherited zircon ages from a diorite xenolith of the Popes Harbour Dyke, Nova Scotia: implications for Late Ediacaran Arc magmatism in the Avalon Terrane of the Northern Appalachians. Minerals 12. https://doi.org/10.3390/min12050575.
Shellnutt, J.G., Owen, J.V., Yeh, M.-W., Dostal, J., Nguyen, D.T., 2019. Long-lived association between Avalonia and the Meguma terrane deduced from zircon geochronology of metasedimentary granulites. Sci. Rep. 9, 4065. https://doi.org/10.1038/s41598-019-40673-9.
Shervais, J.W., 2022. The petrogenesis of modern and ophiolitic lavas reconsidered: Ti-V and Nb-Th. Geosci. Front. 13, 101319 https://doi.org/10.1016/j.gsf.2021.101319.
Silva, J.B., Oliveira, J.T., Ribeiro, A., 1990. Structural outline. In: Dallmeyer, R.D., Garcia, E.M. (Eds.), Pre-Mesozoic Geology of Iberia. Springer, Berlin, pp. 348–362. https://doi.org/10.1007/978-3-642-83980-1_24.
Silva, J.B., Oliveira, J.M., Matos, J., Leitão, J.C., 1997. Aljustrel and the Central Iberian Pyrite Belt. In: Geology and VMS Deposits of the Iberian Pyrite Belt, SEG Neves Corvo Field Conference, pp. 73–124.
Simpson, K., McPhie, J., 2001. Fluidal-clast breccia generated by submarine fire fountaining, Trooper Creek Formation, Queensland, Australia. J. Volcanol. Geotherm. Res. 109, 339–355. https://doi.org/10.1016/S0377-0273(01)00199-8.
Söderlund, U., Johansson, L., 2002. A simple way to extract baddeleyite (ZrO 2). Geochem. Geophys. Geosyst. 3, 1–7. https://doi.org/10.1029/2001GC000212.
Solá, A.R., Salgueiro, R., Pereira, Z., Matos, J.X., Rosa, C., Araújo, V., Neto, R., Lains Amaral, J., 2015. Time span of the volcanic setting of the Neves-Corvo VHMS deposit. In: X Congresso Ibérico de Geoquímica: XVIII Semana de Geoquímica. Laboratório Nacional de Energia e Geologia, pp. 122–125.
Spencer, C.J., Kirkland, C.L., Taylor, R.J.M., 2016. Strategies towards statistically robust interpretations of in situ U–Pb zircon geochronology. Geosci. Front. 7, 581–589. https://doi.org/10.1016/J.GSF.2015.11.006.
Sun, S., McDonough, W.F., 1989. Chemical and isotopic systematics of oceanic basalts: implications for mantle composition and processes. Geol. Soc. Lond. Spec. Publ. 42, 313–345.
Thiéblemont, D., Pascual, E., Stein, G., 1997. Magmatism in the Iberian Pyrite Belt: petrological constraints on a metallogenic model. Mineral. Deposita 33, 98–110. https://doi.org/10.1007/s001260050135.
Tornos, F., 2006. Environment of formation and styles of volcanogenic massive sulfides: the Iberian Pyrite Belt. Ore Geol. Rev. 28, 259–307. https://doi.org/10.1016/J.OREGEOREV.2004.12.005.
Tornos, F., Casquet, C., Relvas, J.M.R.S., 2005. 4: Transpressional tectonics, lower crust decoupling and intrusion of deep mafic sills: a model for the unusual metallogenesis of SW Iberia. Ore Geol. Rev. 27, 133–163.
Tornos, F., Conde, C., Chiaradia, M., Velasco, F., 2015. Evolving subduction-related basins control the formation of VMS deposits in the Iberian Pyrite Belt, in: Society of Economic Geology Conference.
Valenzuela, A., Donaire, T., González-Roldán, M.J., Toscano, M., Pascual, E., 2011a. Volcanic architecture in the Odiel river area and the volcanic environment in the Riotinto–Nerva Unit, Iberian Pyrite Belt, Spain. J. Volcanol. Geotherm. Res. 202, 29–46. https://doi.org/10.1016/j.jvolgeores.2010.12.018.
Valenzuela, Alfonso, Donaire, T., Pin, C., Toscano, M., Hamilton, M.A., Pascual, E., 2011b. Geochemistry and U–Pb dating of felsic volcanic rocks in the Riotinto–Nerva unit, Iberian Pyrite Belt, Spain: crustal thinning, progressive crustal melting and massive sulphide genesis. J. Geol. Soc. Lond. 168, 717–732. https://doi.org/10.1144/0016-76492010-081.
Van Staal, C.R., Whalen, J.B., Valverde-Vaquero, P., Zagorevski, A., Rogers, N., 2009. Pre-carboniferous, episodic accretion-related, orogenesis along the Laurentian margin of the northern Appalachians. Geol. Soc. Spec. Publ. https://doi.org/10.1144/SP327.13.
Vermeesch, P., 2018. IsoplotR: a free and open toolbox for geochronology. Geosci. Front. 9, 1479–1493. https://doi.org/10.1016/j.gsf.2018.04.001.
Vermeesch, P., 2021a. On the treatment of discordant detrital zircon U–Pb data. Geochronology 3, 247–257. https://doi.org/10.5194/gchron-3-247-2021.
Vermeesch, P., 2021b. Maximum depositional age estimation revisited. Geosci. Front. 12, 843–850. https://doi.org/10.1016/j.gsf.2020.08.008.
Vermeesch, P., Pease, V., 2021. A genetic classification of the tholeiitic and calc-alkaline magma series. Geochem. Perspect. Lett. 19, 1–6.
Vervoort, J.-D., Kemp, A.-I., Fisher, C.-M., 2018. Hf isotope constraints on evolution of the depleted mantle and growth of continental crust. In: AGU Fall Meeting Abstracts (pp. V23A-07).
von Raumer, J.F., Nesbor, H.-D., Stampfli, G.M., 2017. The north-subducting Rheic Ocean during the Devonian: consequences for the Rhenohercynian ore sites. Int. J. Earth Sci. 106, 2279–2296. https://doi.org/10.1007/s00531-016-1425-x.
Waldron, J.W.F., White, C.E., Barr, S.M., Simonetti, A., Heaman, L.M., 2009. Provenance of the Meguma terrane. Rifted margin of early Paleozoic Gondwana. Can J Earth Sci, Nova Scotia. https://doi.org/10.1139/E09-004.
Wang, D., Wang, X.-L., Cai, Y., Goldstein, S.L., Yang, T., 2018. Do Hf isotopes in magmatic zircons represent those of their host rocks? J. Asian Earth Sci. 154, 202–212. https://doi.org/10.1016/j.jseaes.2017.12.025.
Wang, D.-B., Wang, B.-D., Yin, F.-G., Sun, Z.-M., Liao, S.-Y., Tang, Y., Luo, L., Liu, Z., 2019. Petrogenesis and tectonic implications of Late Mesoproterozoic A1- and A2-type felsic lavas from the Huili Group, southwestern Yangtze Block. Geol. Mag. 156, 1425–1439. https://doi.org/10.1017/S0016756818000882.
Wang, K., Plank, T., Walker, J.D., Smith, E.I., 2002. A mantle melting profile across the Basin and Range, SW USA. J. Geophys. Res. Solid Earth 107, ECV 5-1–ECV 5-21. https://doi.org/10.1029/2001JB000209.
Whalen, J.B., Currie, K.L., Chappell, B.W., 1987. A-type granites: geochemical characteristics, discrimination and petrogenesis. Contrib. Mineral. Petrol. 95, 407–419. https://doi.org/10.1007/BF00402202.
Winchester, J.A., Floyd, P.A., 1977. Geochemical discrimination of different magma series and their differentiation products using immobile elements. Chem. Geol. 20, 325–343. https://doi.org/10.1016/0009-2541(77)90057-2.
Yang, J.-H., Wu, F.-Y., Chung, S.-L., Wilde, S.A., Chu, M.-F., 2006. A hybrid origin for the Qianshan A-type granite, northeast China: geochemical and Sr–Nd–Hf isotopic evidence. Lithos 89, 89–106. https://doi.org/10.1016/j.lithos.2005.10.002.
Yesares, L., Piña, R., González-Jiménez, J.M., Sáez, R., Ruíz de Almodóvar, G., Fanlo, I., Manuel Pons, J., Vega, R., 2023. Distribution of critical metals in evolving pyrite from massive sulfide ores of the Iberian Pyrite Belt. Ore Geol. Rev. 153, 105275 https://doi.org/10.1016/j.oregeorev.2022.105275.
Zengqian, H., Liquan, W., Zaw, K., Xuanxue, M., Mingjie, W., Dingmou, L., Guitang, P., 2003. Post-collisional crustal extension setting and VHMS mineralization in the Jinshajiang orogenic belt, southwestern China. Ore Geol. Rev. 22, 177–199. https://doi.org/10.1016/S0169-1368(02)00141-5.
Zindler, A., Hart, S., 1986. Chemical geodynamics. Annu. Rev. Earth Planet. Sci. 14, 493–571. https://doi.org/10.1146/annurev.ea.14.050186.002425.